Fall 1-31-2001

Deposition of tantalum on steel by sputtering

Bhavin Shah
New Jersey Institute of Technology

ABSTRACT

DEPOSITION OF TANTALUM ON STEEL BY SPUTTERING

by
Bhavin Shah

Recent interest in tantalum deposition comes from two different applications. One is in microelectronics where thin tantalum films (< 1 μm) are used as diffusion barrier layers for copper interconnects. The other involves its application as a material for corrosion and wear resistant coating on surfaces that are subjected to high stresses and harsh chemical and erosive environments.

This thesis is a part of the investigation done at the Ion Beam and Thin Film Research Laboratory at NJIT to study the deposition conditions and properties of tantalum thin films. It includes the design and construction of Planar D.C. Magnetron Sputtering System and Cylindrical D. C. Magnetron Sputtering System for deposition on the planar and cylindrical surfaces of steel, respectively. The electrical characteristics of the cylindrical system were tested in a range of pressures and conditions for initiation and maintaining of discharge were established.

The successful completion of planar magnetron system was demonstrated by deposition of tantalum films. The quality of these films has improved with refining of the deposition system and the process procedure.

Tantalum films deposited in the planar magnetron sputtering system had thickness in the range of 4000 Å - 6000 Å. As a part of a pilot study, the films were analyzed using profilometry, Scanning Electron Microscope (SEM), X-ray Diffraction (XRD) and Rutherford Backscattering Techniques (RBS).

The characteristics of the films were strongly dependent on the surface preparation and the residual gas in the deposition chamber. The presence of oxygen and water vapor in the residual gas results in films containing substantial amount of oxygen. Proper cleaning of steel substrates is essential for film integrity and adhesion. Surface preparation, including steel polishing, also influences crystallinity of the films. Typically, alpha and beta tantalum phases are present but there are indications that under controlled conditions pure alpha phase can be formed.

DEPOSITION OF TANTALUM ON STEEL BY SPUTTERING

by
Bhavin Shah

A Thesis
Submitted to the Faculty of
New Jersey Institute of Technology
in Partial Fulfillment of the Requirements for the Degree of
Master of Science in Materials Science and Engineering

Interdisciplinary Program in Materials Science and Engineering

January 2001

APPROVAL PAGE

DEPOSITION OF TANTALUM ON STEEL BY SPUTTERING

Bhavin Shah

Dr. Marek Sosnowski, Thesis Advisor — Date
Associate Professor, Department of Electrical and Computer Engineering, NJIT.

Dr. Roland A. Levy, Committee Member — Date
Distinguished Professor, Department of Physics, NJIT.

Dr. Trevor Tyson, Committee Member — Date
Associate Professor, Department of Physics, NJIT.

BIOGRAPHICAL SKETCH

Author: Bhavin Shah

Degree: Master of Science

Date: January 2001

Undergraduate and Graduate Education:

- Master of Science in Materials Science and Engineering
  New Jersey Institute of Technology, Newark, NJ, 2001

- Bachelor of Engineering in Metallurgical Engineering
  Maharaja Sayajirao University, Baroda, India, 1998

Major: Materials Science and Engineering

Papers Presented:

Bharat Chauhan, Bhavin Shah, Pinakin Jaiswal
"Modeling in Metallurgy with a Special Reference to Martensitic Micro Structural Modeling", at International Conference held by IPCL, Baroda, India, 1998.

Bhavin Shah, Naresh Wadhwani
"Advanced Ceramics", at Regional Engineering College, Rourkela, Orissa, India, 1996.

This work is dedicated to my
beloved parents and sister

ACKNOWLEDGEMENT

Words fail to express my gratitude and appreciation to Dr. Marek Sosnowski, who gave me opportunity of working under his supervision during my graduate study at NJIT, and served as my research advisor. I am extremely thankful to him not only for his patience and understanding, but also for his expert guidance and invaluable suggestions. I also appreciate his questions and recommendations, which made this work and my educational goals more meaningful. I have learned from him not only academically but also in other general aspects of life.

I am also highly grateful to Dr. Trevor Tyson and Dr. Roland A. Levy for serving as members of the committee.

My fellow students at the Ion Beam and Thin Film Research Laboratory, Anamika Patel, Maria Albano, Cheng Li and Younes Abbassi deserve a word of appreciation for their constant support and help. Special recognition also goes to Mr. John Hoinowski for his help in machining components for the system.

I would also like to thank Minal Shah, Mahesh Ajgaonkar, Kiran Shah, Sanket Shah, Chirag Morakhia and Mihir Tungare who made the period of this work a pleasant one.

Special recognition also goes to Anto Yohannan for doing the characterization of films and as a helping me as a co-worker.

This research was funded in parts by a grant provided by the US Army.

TABLE OF CONTENTS

TABLE OF CONTENTS
(Continued)

LIST OF TABLES

LIST OF FIGURES

LIST OF FIGURES
(Continued)

LIST OF FIGURES
(Continued)

CHAPTER 1

INTRODUCTION

The main aim of this research project was to study the deposition process and properties of tantalum films deposited by sputtering. Most of the investigations of tantalum films have been carried out using films deposited by sputtering because of the relative ease with which films of refractory metals can be sputtered in comparison with other techniques. Sputtering is widely used to deposit refractory metals like tantalum, titanium, tungsten and niobium, which would require very high temperatures for deposition, by evaporation. Electron beam evaporation is the only technique, which would allow the later. Sputtering is a universal deposition method, which is also used for deposition of lower melting point metals like copper and aluminum [1].

Tantalum is most widely used in the electronic industry and as a protective coating in many industries because of its good resistance to erosion. An extensive interest in the electrical and structural properties of tantalum as a thin film material has been stimulated over the past twenty-five years by its use in the microelectronics industry. With a melting point of around 3000 °C stable films of tantalum may be produced despite the presence of defects or impurities [2].

In the current IC generations where the effective size of devices are below 0.18 μm, Cu has been introduced as an interconnect metal. But Cu readily diffuses through SiO_2 and then into the silicon lattice where it creates deep impurity levels and reduces transistor performance. To counteract this problem Tantalum and Tantalum Nitride is extensively used as a diffusion barrier layer in the modern semiconductor industry [3].

While pure copper on Si reacts at 200 °C, the Ta films prevent Cu silicon interaction upto 600 °C [4].

Sputtered tantalum films are widely used in the microelectronics industry as the films can be reactively sputtered and thus resistivity and temperature coefficient of resistance can be controlled [5]. Sputtered tantalum can be also be used as an effective corrosion resistance barrier if the coating is continuous, defect free and is adherent to the substrate it is intended to protect [6]. Chromium is deposited onto gun barrels by electroplating. It is typically electroplated from its hexavalent form, which is a carcinogen and thus difficult to handle and has an adverse environmental effect [7]. Moreover, chromium deposited steel cannot be recycled easily, because of adverse environmental problems. Properties of various refractory metals such as tantalum, molybdenum, niobium and tungsten indicate that these materials can exhibit superior resistance to erosion processes, which occur at gun tube surfaces. Testing of tantalum coated steel liners showed less erosion rate then all other liners including chromium coated liners. To avoid degradation of the gun tube mechanical properties, thick tantalum coatings may be applied to the inner tube surface with high rate sputtering deposition [8].

The refractory nature and high ductility of body centered cubic (bcc) phase tantalum makes it a suitable material for corrosion and wear resistant coatings on surfaces that are subjected to high stresses and harsh chemical and erosive environments [9].

This thesis contains information pertaining to the work carried out at the Ion Beam and Thin Film Research Laboratory at NJIT, on the design and construction of the planar dc magnetron sputtering system and cylindrical magnetron sputtering system, for

investigating the properties of tantalum films deposited on the inner surface of steel tubes.

This work started in a joint collaboration of U. S. Army Industrial Ecology Center, New Jersey Institute of Technology, National Defense Center for Environmental Excellence (NDCEE) and New Mexico State University.

The main objective of the research were:

1) To design and construct the planar and cylindrical magnetron sputtering system
2) To study the properties of tantalum films and their dependence on deposition parameters.

In the first phase of the project tantalum films in the range of 4000 Å - 6000 Å were deposited in the planar deposition system and the operation of the cylindrical system was studied with a copper target. In the next phase, there are plans to deposit tantalum films with 100 μm thickness in the planar system. Also with proper plasma control and pumping the copper target in the cylindrical system would be replaced with a tantalum target to deposit on the inner surface of steel tube.

Chapter 2 deals with the properties and application of tantalum both in microelectronics and as a protective barrier. Chapter 3 describes sputtering as a deposition technique. Description of the planar dc magnetron sputtering system is given in Chapter 4. It also explains the mounting of the substrate inside the deposition system, testing of the deposition system and deposition parameters. Chapter 5 describes the cylindrical magnetron sputtering system. It explains the principle of the system and problems of plasma control. Chapter 6 explains the analysis of the films by techniques

like SEM, XRD and RBS. Summary and conclusion during the course of this thesis are discussed in Chapter 7.

CHAPTER 2

PROPERTIES AND APPLICATIONS OF TANTALUM

2.1 Physical Properties

Tantalum a group V transition metal is grayish silver in color and heavy with a density of 16.6 gcm^{-3}. It is a refractory metal with a melting point of 2996.0 °C. It's a hard metal with a Brinell Hardness of 800 MN/m^2. Heat of vaporization and heat of fusion are 743 and 31.6 kJ/mol respectively [10]. In pure form, it is ductile and can be drawn into fine wire. It is immune to chemical attacks at temperatures below 150 °C. A transition to the superconducting state is recorded at 4.4 °K [11]. It has two crystalline forms viz. body centered cubic (commonly known as alpha-tantalum) and tetragonal metastable phase (commonly known as beta-tantalum). The b.c.c tantalum commonly found in bulk has a resistivity of 15-60 $\mu\Omega$cm whereas beta tantalum found in thin films of tantalum has an as-deposited resistivity of 170-210 $\mu\Omega$cm [2][12]. Corresponding temperature coefficients of resistance are +500 to +1800 and –100 to +100 p.p.m / °C.

2.2 Crystal Structure

Two most common crystalline structures recognized in thin films of tantalum are:

1) body centered cubic (α - Ta); a_o = 3.3-3.4 Å
2) tetragonal (β - Ta); a_o = 5.3 °A, c = 9.9-10 Å

There are also reports of other structures of tantalum found like the face centered cubic with an a_o = 4.4-4.5 Å which is a metastable phase and the omega phase of tantalum [2].

In bulk, tantalum has the b.c.c. crystalline structure with a lattice parameter of 3.303 Å. However, depending upon the deposition technique used, the as-deposited crystal structure can also be b.c.c. alpha phase or a mixture of beta and alpha phase tantalum [2][6]. The crystal structure of as deposited tantalum films contains usually the metastable tetragonal beta phase [12]. Beta tantalum spontaneously reverts to the bcc phase at temperatures between 750 and 800 °C.

Films with b.c.c. structure are formed as a randomly oriented material or with either the (111) or (110) plane parallel to the substrate [13]. β – Ta has always been found with the (100) plane preferentially oriented parallel to the substrate [3].

The reasons for the formation of beta tantalum and the structure of beta tantalum are not clearly resolved. According to Read and Atlmann, who discovered β - Ta in 1965 at Bell Laboratories, the new tantalum phase is formed only in very pure sputtering atmosphere [14]. Work by Westwood and Livermore of Bell Northern Research shows that β – Ta is formed to accommodate extra gas when the solubility limit is exceeded for the b.c.c. phase [15]. However, work by Croset and Velasco shows that the formation of β – Ta does not depend on the gas content but on sputtering power and/or substrate temperatures [16].

According to other investigators, formation of β - Ta is caused either by impurity atoms adsorbed at the surface or by reactive gases added to the sputtering atmosphere. The presence on the substrate surface of O or OH formed by reaction of H_2O with the surface oxide, is necessary for the nucleation of β – Ta, but the presence of impurities is not necessary during the growth stage [17][18]. However studies done by Sato shows that pure b.c.c phase is yielded when films were deposited onto Ta_2O_5 and SiO_2 substrates. Therefore the reason for the formation of β – Ta may be related to the difference between

the deposition rates of tantalum atoms by magnetron sputtering and a conventional d.c. sputtering or to the substrate heating during deposition. In addition, the crystal structure of the substrate may be an important factor in defining the b.c.c. structure in bulk tantalum [19].

The physical picture of the β – Ta crystalline structure is such that tantalum atoms are tightly packed in a hexagonal array within each layer [22]. Since both d.c. and r.f. magnetron sputtering can achieve deposition rates an order of magnitude higher than a conventional d.c. sputtering with a relatively low substrate temperature, the packing forces for tantalum atoms in the sputtering may partially dominate the b.c.c. structure-defining electronic forces with the resultant formation of β phase [19].

Marcus and Quigley [21] and Denbigh and Marcus [22] (both used an electron beam evaporation technique) have reported f.c.c. phase as a phase stable only up to approximately 100 Å thick film. For each deposition technique there has been a critical substrate temperature range for f.c.c. formation outside which the b.c.c or an amorphous phase has been produced. The increase in the lattice constant of b.c.c. tantalum in thin films over that of the bulk material is likely due to the inclusion of impurities in the film during the deposition process [2]. This is because the b.c.c-Ta can incorporate considerably larger amounts of reactive gases than β-Ta without changing its structure [13].

A b.c.c. based super lattice structure with slight tetragonal distortion has been observed by Das for films d.c. and r.f. sputtered with a negative bias. Experimental values for the lattice constants are a = b = 10.29 Å and c = 9.2 Å [23].

An investigation on the deformation substructure developed within shock-loaded tantalum by TEM has revealed that a phase change can also take place in tantalum under

a high shock pressure (45 Gpa). A b.c.c. - ω (hexagonal) displacive transformation is observed in tantalum. Needle- or plate-like ω phase is found to form accompanied with the {112} type deformation twins within shock-recovered tantalum [24].

Although much work has been performed on beta tantalum, the detailed structure of beta tantalum is still not well understood.

2.3 Applications

With the current trend of IC generations below 0.18 μm, Cu is being introduced as an interconnect metal. But Cu readily diffuses through SiO_2 and then enters silicon lattice, where it creates deep impurity levels that degrade transistor performance and cause junction leakage. Also unlike Al, Cu does not adhere well to SiO_2. To counteract these problems materials like Ta / TaN and TiN are used as liners under Cu lines. Ta is an attractive barrier material because of its high melting point and immiscibility with Cu. It also forms strong metal-metal bonds. Thus, it provides a low-resistance ohmic contact and excellent adhesion to copper above and below it. Doping the Ta with a few percent of nitrogen blocks the grain boundary diffusion paths. More heavily nitrided Ta, produced by reactive sputtering of Ta in the presence of nitrogen, can also be used as a barrier layer [3].

Low resistivity α – Ta has applications in thin film capacitors to achieve higher frequency performance [25]. The thickness of Ta films used, as a base material for thin film capacitors is usually approximately 400nm [18].

The refractory nature and high ductility of body centered cubic (bcc) phase tantalum makes it a suitable material for corrosion and wear resistant coatings on surfaces that are subjected to high stresses and harsh chemical and erosive environments [9].

Sputtered tantalum can be used as an effective corrosion resistance barrier if the coating is continuous, defect free and is adherent to the substrate it is intended to protect [4]. Presently the useful life of various gun tubes is increased by protecting the internal gun tube surface with electro deposited chromium. Chromium may soon be replaced by tantalum in this application.

Though a highly expensive material used for special applications, since it has a high degree of ductility and malleability, almost any equipment design can be constructed from tantalum. Typical product examples are reactor vessels, columns, bayonet heaters, and tube condensers or heater exchangers, lined piping, valves, thermowells, spargers, rupture disks, glass repair kits, filaments for light bulbs, canalization for switches of liquid metals in nuclear reactors, surgical instruments and implants. Tantalum also has many applications in pharmaceutical plants. Tantalum products are preferred because they resist corrosion and preserve product purity [26].

CHAPTER 3

SPUTTERING AS A DEPOSITION TECHNIQUE

3.1 Introduction

A large variety of "thin films" are used in today's industry for the fabrication of various microelectronic, optical and bioengineering devices. The formation of such films is accomplished by a variety of techniques, which can be divided into three groups:

1) films grown by interaction of a vapor-deposited species with the substrate
2) film formation by deposition without causing changes to the substrate material and
3) coating of the substrate with a liquid, which is then dried to form the solid thin film.

The first category includes thermal oxidation and nitridation of single crystal and polysilicon. The second group includes two subclasses of deposition. The first of these is chemical vapor deposition (CVD), in which films are formed by chemical reaction of vapor phase chemicals that contains the required constituent. The second is physical vapor deposition (PVD), in which the species of the thin film are physically dislodged from a source and transported to the substrate to form a thin film. The formation of thin films by PVD includes the processes of sputtering and evaporation. The deposition of a liquid on a substrate to form thin films is most commonly done by spin coating [2].

Films of refractory materials can also be deposited by pulsed laser deposition (PLD). In this technique a high power UV laser operating at repetition rate of 10 Hz to 1 kHz focused on a target of the material which is deposited as thin film. The substrate is located in close proximity to the target. The laser pulses used are of very short duration ranging from few nano seconds to few femto seconds. A set of optical components is used to focus and raster the laser beam over the target surface. Alternatively a fixed laser

beam is used with a rotary target. Film growth can be carried out in vacuum or in a reactive gas, at pressures greater than 10 mTorr. This technique can be used to deposit highly pure films with a good thickness control. Other advantages of PLD include its versatility to deposit stoichiometric compound films like GaAs, ZnO, Fe_2O_3, GeO_2. Unlike sputtering PLD can be also be used to grow epitaxial films and hetero-structures at low cost [27][28].

3.2 Physical Vapor Deposition Methods

3.2.1 Sputtering

Sputtering is a process in which atoms are ejected from the surface of a material (i.e. target) when that surface is struck by sufficiently energetic particles (i.e. ions). From this definition, sputtering can be considered as an etching process and is used for surface cleaning and for pattern delineation. Since sputtering removes and transports the target material, it is also used as a method of film deposition. It has become the dominant technique for depositing a variety of metallic films in VLSI and ULSI fabrication, including aluminum alloys, titanium, titanium:tungsten, titanium nitride, tantalum and cobalt [3] [29]. Sputtering can further be classified as follows:

1) Diode sputtering
2) Bias sputtering (ion plating)
3) Magnetron sputtering
4) Ion beam sputter deposition

Sputtering largely displaced the original PVD technique of evaporation for depositing thin films for following reasons:

1) Sputtering can be accomplished from large area target.

2) The alloy composition of sputter deposited films can be more easily controlled than that of evaporated films.
3) Important film properties, such as step coverage and grain structure can be controlled by varying the negative bias and heat applied to the substrate.
4) Film thickness is relatively easily controlled by selecting a constant set of operating conditions [3].

Sputtering also has its drawbacks:

1) The capital expenditure for sputtering equipment is high.
2) It's too slow for some applications of coating.
3) Better step coverage can generally be achieved by CVD [3].

3.2.2 Applications of Sputtering

1) SPUTTER ETCHING

Sputtering process essentially involves knocking out atoms of the surface of a target by the impact of ions. This leads to the removal of material or etching of the target. The technique can also be used to generate surface topography, or surface patterns, by selectively protecting a part of the surface of the target material during the sputter etch.

2) SPUTTER DEPOSITION

The ejected atom can under the right circumstances, move through the space until it strikes and deposits on the surface of a receiver, which is known as a substrate. At sufficient bombarding ion energy and current a coating of several or many atomic layers of target material can be built on the substrate. This process of film deposition is known as sputter deposition [29].

3.2.3 Sputtering of Metals

Sputtering is largely used to deposit various kinds of materials like aluminum, gold, titanium. In microelectronics it is used to deposit critical barrier layers like Ta, TaN or TiN and the Cu seed layer (sputtered Cu). For Al – based metallization, novel approach as ionized magnetron sputtering or I-PVD, wherein a large fraction of the neutral sputtered flux is ionized while being transported to the substrate, is used to create barrier/liner layers in high aspect ratio contacts and vias. The deposition of Ti and Co for silicide processes is also performed by sputtering [3].

Sputtering can be done using ions of noble gases like argon and krypton where there is no chemical reaction between the sputtering gas and the target. When reactive gases are introduced into the sputtering chamber during the deposition process, wherein the gases react with the ejected target atoms, compound films are deposited by sputtering. This process is termed as reactive sputtering. The main application of reactive sputtering in microelectronics fabrication involves in the sputter deposition of the barrier film material TiN.

By using multi-component targets, alloy film like Al:Cu or Ti:W can also be deposited by sputtering [3].

3.2.4 Mechanism of Sputtering

As shown in Fig. 3.1 when an energetic ion approaches the surface of a solid (target) one or all of the following phenomena may occur:

- The ion may be reflected, being getting neutralized in the process.
- The impact of the ion may cause the target to eject an electron, called the secondary electron.
- The ion may become buried in the target.
- The ion impact might be responsible for some structural changes in the target material.
- The ion impact may set up a series of collisions between atoms of the target, leading to the ejection of one of the target atoms. This ejection process is known as sputtering [30].

The principles of sputtering can be understood using a relatively simple momentum transfer model. Using this model it is possible to visualize how atoms are ejected from a surface as a result of two binary collisions. The sputtering process is often compared to the game of atomic billiards as shown in Fig. 3.2 in which the cue ball (the bombarding ion) strikes the neatly arranged pack (atomic array of target), scattering balls (target atoms) in all directions, including some back towards the target [3].

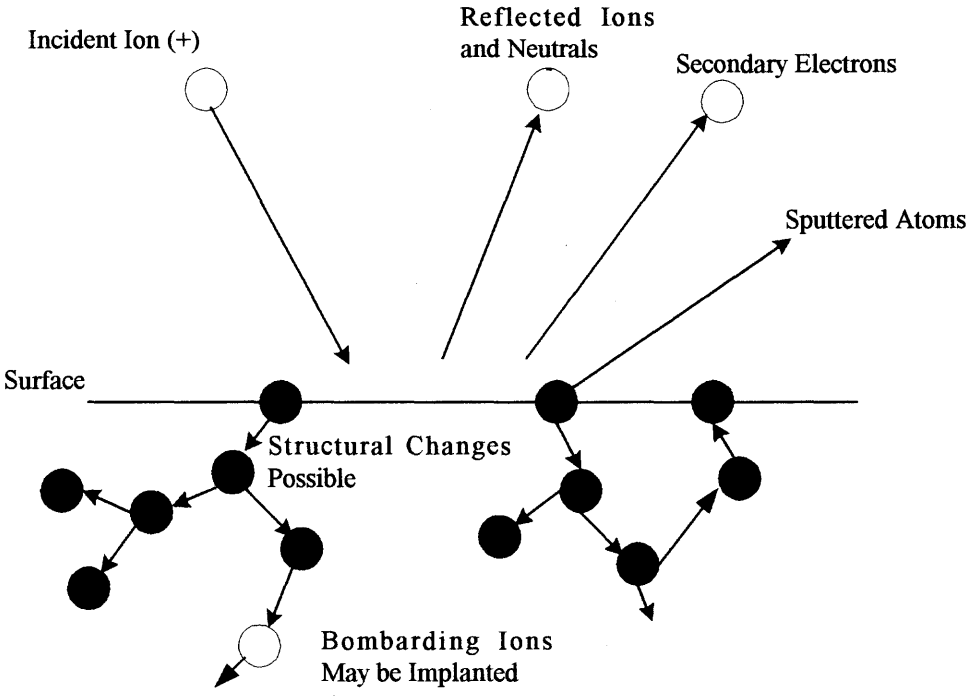

Fig 3.1 Interaction of ions with surfaces (Ref. Brian Chapman)

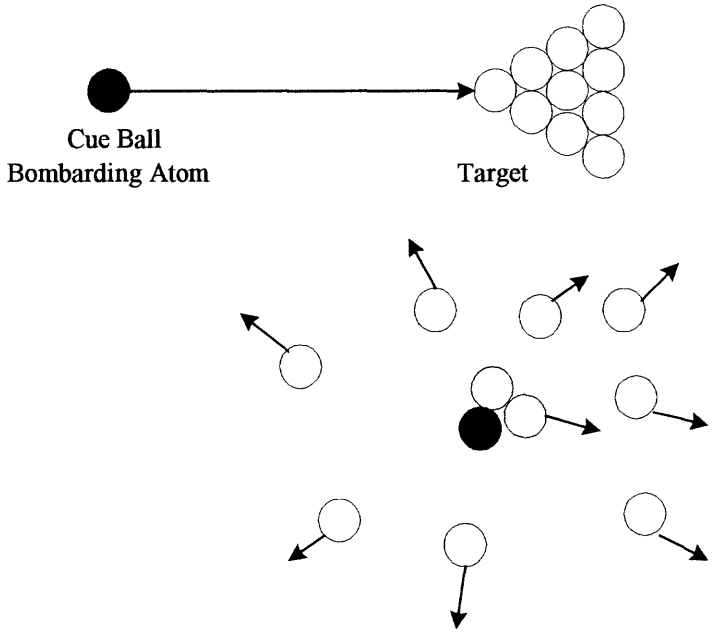

Fig 3.2 Sputtering – the atomic billiards game (Ref. Brian Chapman)

The series of collisions in the target, generated by the primary collision at the surface, is known as a collision cascade. It is a matter of probability whether this cascade

leads to the sputter ejection of an atom from the surface (which will require atleast two collisions) or whether the cascade heads off into the interior of the target, gradually dissipating the energy of the primary impact, ultimately to lattice vibration [3]. Sputtering ejection is rather energy inefficient, with typically 1% of the incident energy reappearing as the energy of the sputtered atom [30]. The rest of the energy is lost in the form of heating of the chamber walls, parts inside the chamber and the target.

3.3 Magnetron Sputtering

In a simple d.c. sputtering system the material to be sputtered is made the sputtering target which becomes the cathode of an electrical circuit, and has a high negative voltage V (d.c.) applied to it. The substrate, which is to be coated, is placed on an electrically grounded anode a few inches away as shown in Fig 3.3. These electrodes are kept in a chamber, which is pumped to a high vacuum of $1x10^{-7}$ Torr to $1x10^{-9}$ Torr. Argon gas is introduced into the chamber at a pressure in the range of 30-120 mTorr. The applied electric field created by applying a voltage in the range of 100 V to few kV causes ionization of argon atoms, which creates the glow discharge. Positive ions are accelerated to the target sputtering each atom of the target, which is deposited on the nearby substrate. However the deposition rate of a simple d.c. sputtering system is not very high and hence magnetron sputtering systems are used [30].

Magnetron sputtering uses magnetic fields transverse to the electric field at sputtering target surface [29]. Magnetron sources increase the rate of ionizing collisions by utilizing magnetic fields to help confine the electrons near the target surface. As a result, in magnetron sputtering processes, current densities at the target are 10-100 mA/cm^2, compared to about only 1 mA/cm^2 for dc-diode configurations. In addition

magnetron sources can sustain a glow discharge at much lower pressures than can dc diodes [3].

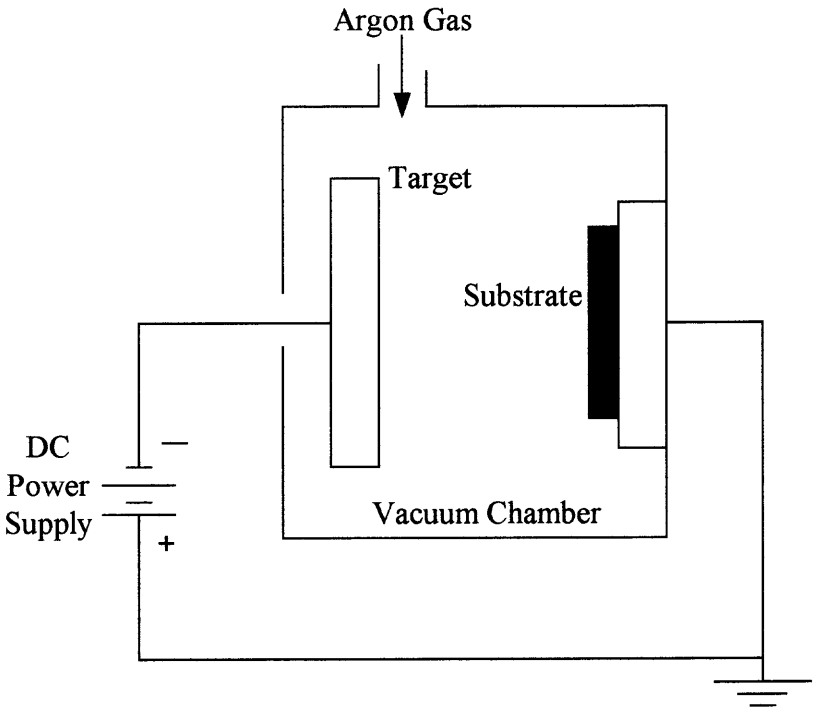

Fig 3.3 Schematic of a dc sputtering system (Ref. Brian Chapman)

The principle of magnetron sputtering can be described by considering the motion of an electron having a charge q, a mass m, and a velocity v. If the electron is moving in a region of uniform magnetic field B (into the paper in Fig 3.4a) and zero electric field, then it experiences a force, F = q (v x B) which is perpendicular to both the direction of its motion and the direction of B. This force F will cause it to move in a circular path with radius r_g, provided it does not collide en route, and return to the surface with velocity v, whose value is given by the equation:

$$r_g = mv / qB$$

For electrons and Ar^+ ions, the equation for r_g can be expressed in terms of the energy, E, of the particles (in eV) and of the magnetic field B (in gauss) as:

$$r_g \text{ (electron)} = 3.37 \times [E^{1/2}(eV) / B \text{ (gauss)}]$$

$$r_g (Ar^+) = 9.11 \times 10^2 [E^{1/2}(eV) / B \text{ (gauss)}]$$

From these equations, it can be seen that Ar^+ ions have motion radii, which are 300 times larger than the radii of electrons for equal values of B and particle energy. Thus the radius of an ion's circular path is so large that it essentially moves in a straight line when crossing the dark space of the cathode. Thus the direction of electron motion is strongly influenced by the magnetic field, which traps the electron near the surface from which it was emitted, while the magnetic field does not significantly change the direction of ions as they cross the dark space.

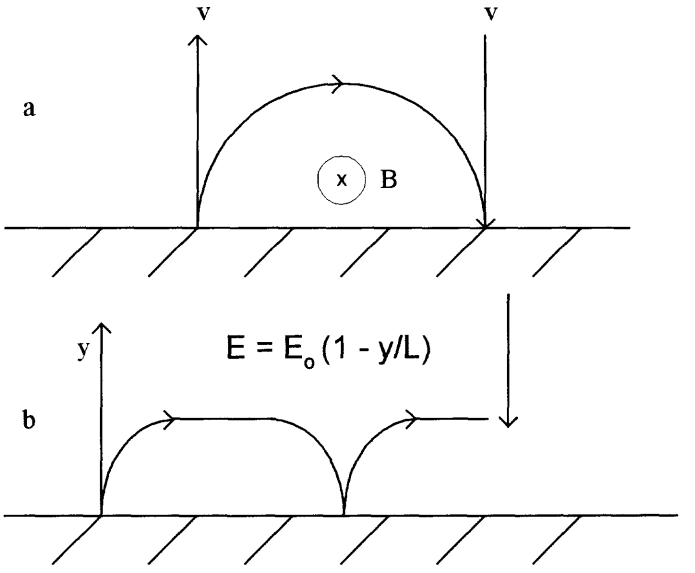

Fig 3.4 Motion of an electron ejected from a surface with velocity v into a region of magnetic field B parallel to the surface:
(a) with no electric field
(b) with a linearly decreasing field. (Ref. Brian Chapman)

To examine a situation more closer to the magnetic sputtering application, Fig 3.4b is of a sputtering target where there is a strong electric field E in the dark space above its surface, and again a magnetic field B parallel to the surface of the target. Let the electric field E decrease linearly across the dark space of thickness L. If y is the dimension away from the target, and the target surface is y = 0, then

$$E = E_o(1 - y/L)$$

where E_o is the field at the target. The electron is then accelerated away from the target in a direction perpendicular to the target surface by the electric field, but it also experiences a force due to the magnetic field, $F = q (v \times B)$.

This force changes the direction of the electron's motion so it is no longer perpendicular to the surface. The addition of the electric field on the target changes the orbits from circular to cycloidal, provided the electron stays within the dark space. As it approaches the target surface after having been deflected, the electron is decelerated by the electric field. Since $r_g = mv / qB$, its instantaneous radius of curvature is decreased as it travels further from the target surface, causing the electron to pivot sharply until it is again moving away from the surface. At that point, the next period of the cycloidal motion is initiated, with the electron again being repelled by the E-field. The net result is that secondary electrons are trapped near the target surface by the combination of the magnetic field and electric fields, and continue to move with a cycloidal motion until they collide with an Ar atom [3][30]. This reduces the loss of electrons going to the anode and walls. Such trapped secondary electrons do not bombard substrates because of the cycloidal motion and thus do not contribute to increased substrate temperature and radiation damage. This allows the use of substrates that are temperature-sensitive with minimum adverse effect. Also magnetron sputtering sources produces higher deposition

rates than conventional sources and hence are widely used in large area industrial applications [29].

3.3.1 Common Configurations of Sputtering System

There are several types of magnetrons for practical applications. The most common configurations are:

1) Planar

In this type of magnetron electrode configuration the target surface is planar, and the B-field is created by permanent magnets behind the targets. This kind of configuration is widely used in torus magnetron sputtering sources. During deposition the substrates are stationary in front of the target. A 'looping' magnetic field is used, and this restricts the sputter erosion of the target to a 'racetrack' area [3].

2) Cylindrical

This type of magnetron systems has a cylindrical geometry and an axial magnetic field. With the inner cylinder as the target, the arrangement is knows as a cylindrical magnetron or post magnetron. This configuration has the ability to coat a large area of small substrates.

When the inside of the chamber becomes the target as shown in Fig. 3.5, the arrangement is known as an inverted magnetron and has a capability of depositing films over strangely shaped substrates placed along the axis [30].

Such type of systems are possible when magnetic field is created from outside. But when steel tube is used as a substrate, magnetic field must be created from inside the system. Such geometry is difficult to achieve and is described later in this work in Chapter 6.

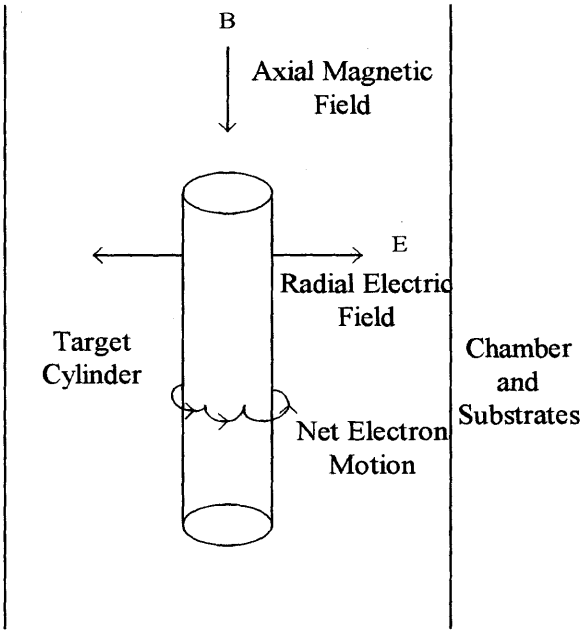

Fig 3.5 Cylindrical magnetron sputtering configuration (Ref. Brian Chapman)

3.4 RF Sputtering

One of the limitations of simple d.c. diode systems is that they cannot sputter insulators (dielectrics). This is due to the fact that glow discharges cannot be maintained with a dc voltage if the electrodes are covered with insulating layers. Hence the technique of r.f. sputtering was developed wherein an ac voltage is applied to the electrodes [3]. AC glow discharges are operated at 13.5 MHz frequency. A magnetic field can also be used with r.f. sputtering to increase the rate of deposition. The introduction of rf sputtering greatly extended the range of utility of the sputter deposition technique and hence sputtering can be used for a wide range of materials [29].

CHAPTER 4

PLANAR DC MAGNETRON SPUTTERING SYSTEM

4.1 Deposition Chamber

The chamber for deposition on planar substrates was designed at the Ion Beam and Thin Film Research Laboratory at NJIT, and fabricated by Kurt J. Lesker company. The chamber is essentially cylindrical in geometry with a volume of approximately 80L. The overall inside dimensions of the chamber is 15" in height and 20" in diameter. This chamber has been designed with the capability of carrying out deposition from more than one source/gun. A photograph of the chamber is shown in Fig 4.1 and the diagram of its main internal components in Fig 4.2.

The chamber is pumped by a mechanical pump to a base pressure of 100 mTorr, after which, it is pumped by a cryo pump to a base pressure of 1.0×10^{-7} Torr. Argon gas pressure during sputtering is measured by a capacitance manometer (MKS Baratron model Type 626) with a range from 0-1 Torr.

Three halogen bulbs are mounted inside the chamber to bake it before sputtering up to a temperature of 200 °C. Residual gases inside the chamber can be analyzed by a residual gas analyzer (RGA) (Inficon Quadrex 200). Tantalum target of 2" dia. and 0.125" thickness and 99.99% purity is mounted on a water-cooled torus magnetron-sputtering gun. The substrates are mounted above the gun facing downwards. This way the particulate or metal flakes which can form on the gun shield or other fixtures are prevented from falling on the substrates.

Fig 4.1 Planar dc magnetron sputtering system

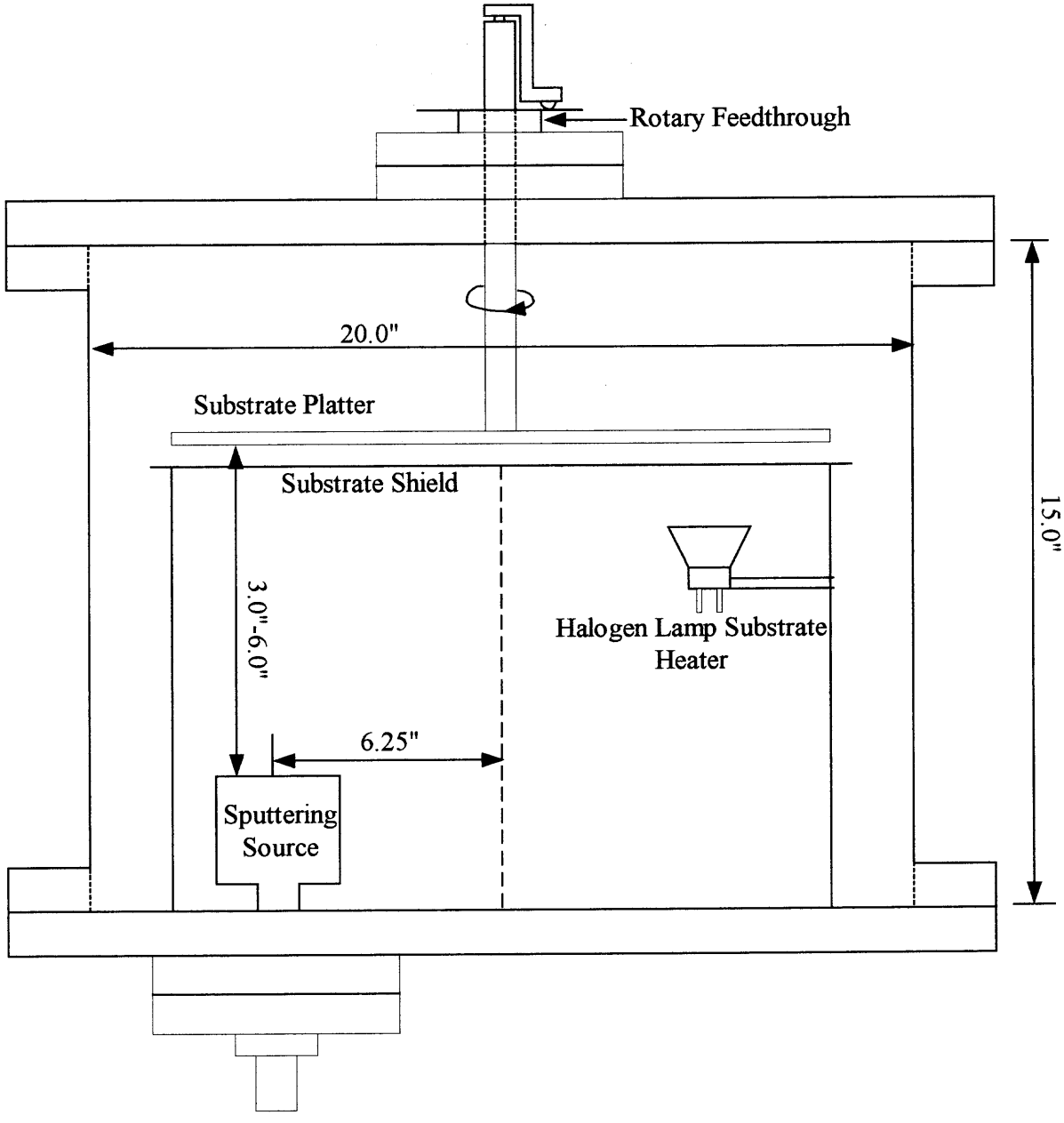

Fig 4.2 Overview of the deposition chamber

4.2 Substrate Mounting

A substrate platter of 16.50" dia. as shown in Fig 4.3 was designed to support the substrate holders to which substrates were attached. This substrate platter has eight openings of 2.75" dia respectively.

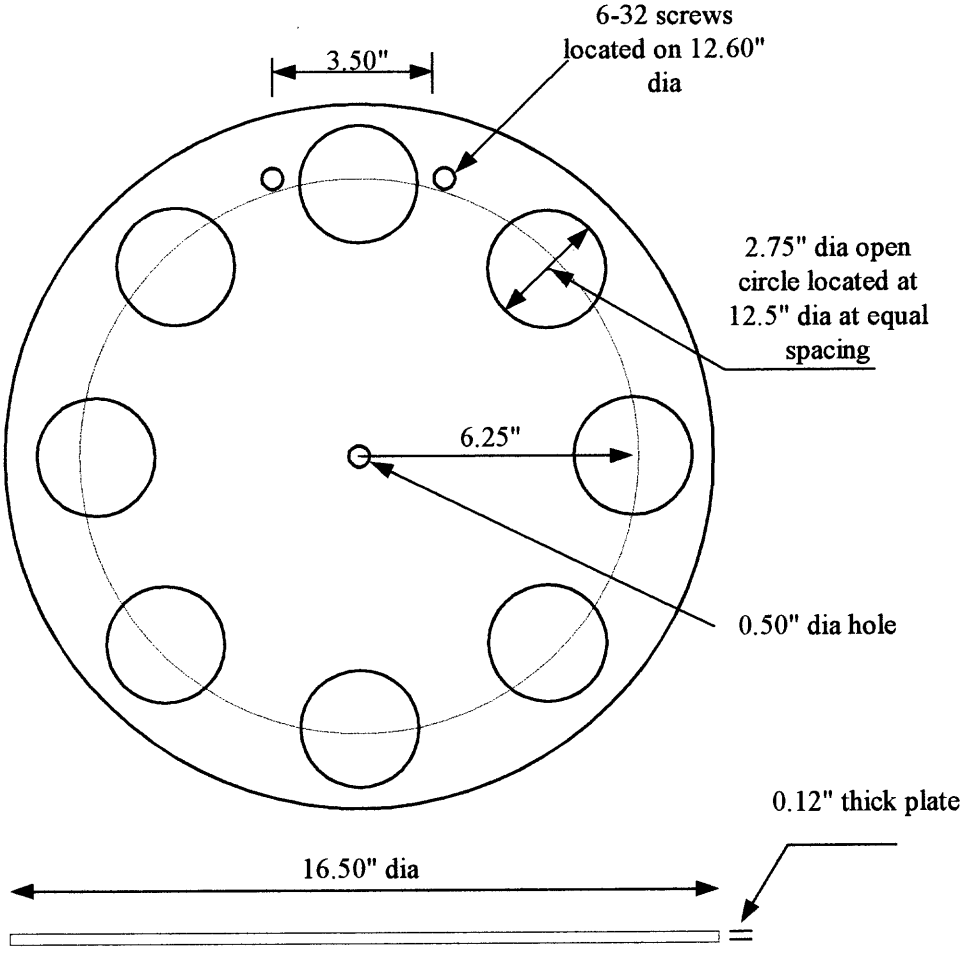

Fig 4.3 Substrate platter

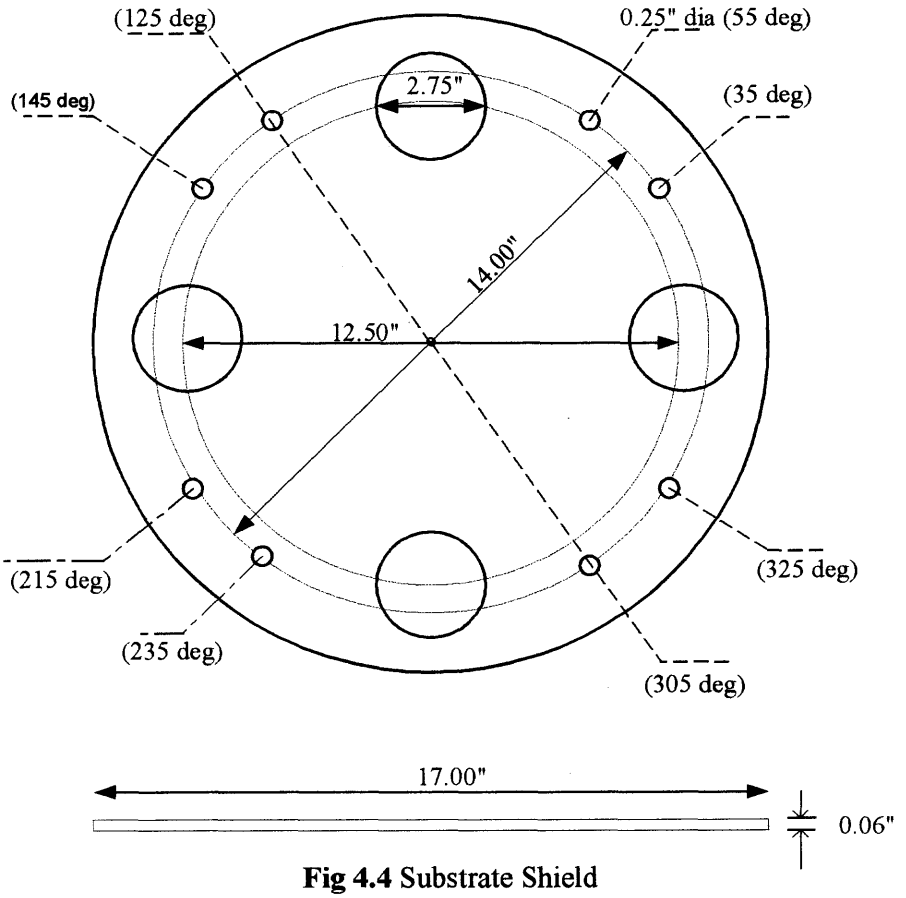

Fig 4.4 Substrate Shield

As shown in Fig 4.5 the platter is mounted on a shaft, which can be rotated from outside the chamber. A substrate shield of 17.00" diameter, shown in Fig 4.4, is supported by four posts mounted on the chamber bottom. The shield protects the substrate platter from the sputtered material.

This substrate shield has four openings of 2.75" dia. each located above the deposition sources. With one sputtering source, initially mounted in the chamber, three shield openings were blocked with blank plugs. This way only one substrate holder at a time can be positioned above the source and the corresponding shield opening, while the other substrate holders are shielded from the deposited material. Rotating the platter shaft by 1/8 at a time brings another substrate holder above the deposition source. Presently

another opening in the shield, opposite from the sputtering source, is used for heating of substrates prior to deposition with halogen lamps.

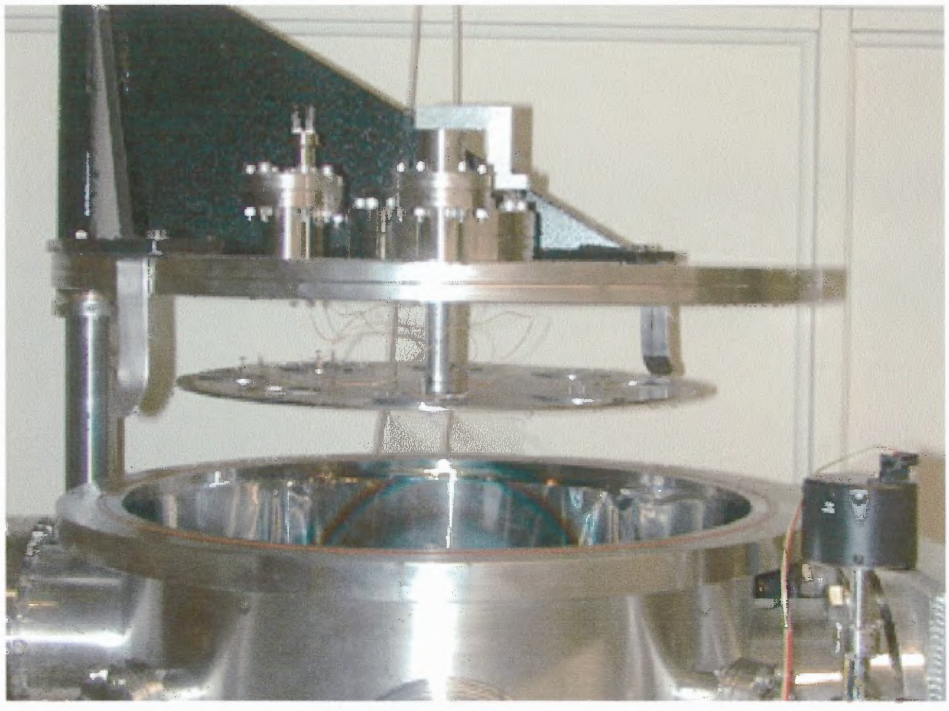

Fig 4.5 Substrate platter mounted on the shaft inside the chamber

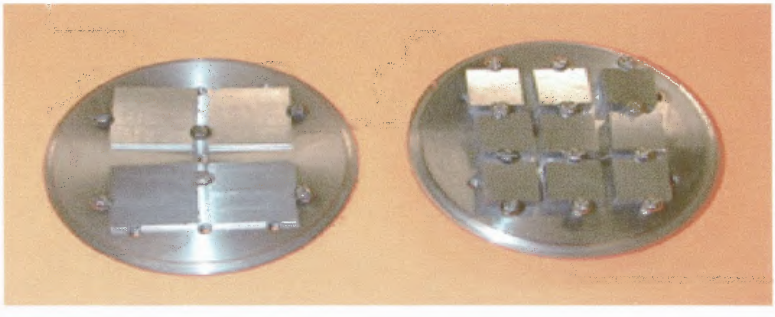

Fig 4.6 Steel samples mounted on substrate holder

As shown in Fig 4.6 two types of steel samples of 0.5"x0.5" and 0.7"x0.7" size were mounted on a specially designed 2.75" diameter substrate mounting plate (substrate

holder). The thickness of the samples was 0.195" and 0.075" respectively. Nine of 0.5" type samples and four of 0.7" type samples can be mounted on the holder at a time as shown in Fig 4.7. The substrates are kept in position by 4-40 screws. The substrate holder is kept in position on the substrate platter by gravity. All parts were fabricated from stainless steel.

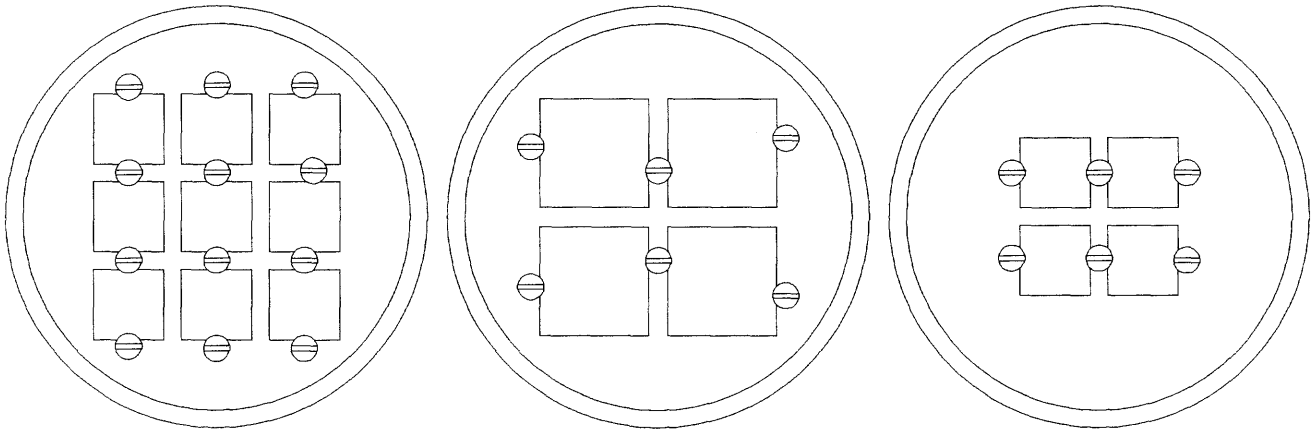

Fig 4.7 Different mounting possibilities for stainless steel samples on substrate

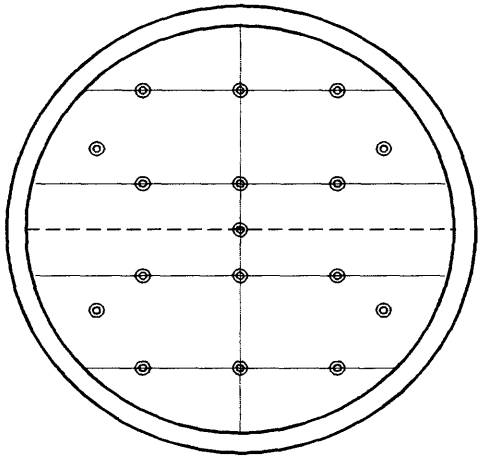

Fig 4.8 Substrate holder with the pattern of threaded hole (4-40) for mounting substrates as shown in Fig 4.7

In order to avoid deposition on the chamber walls additional shield of thin stainless steel is placed above the sputtering source as shown in Fig 4.9.

Fig 4.9 Inner view of the deposition chamber showing sputtering gun and source shield.

The substrates can be heated from the bottom by a halogen bulb (300 W) mounted on one of the four shafts supporting the substrate shield. The distance between the target and the substrate can be adjusted from 3.0" to 6.0".

4.3 Gas Flow Control

A schematic of the gas flow control is shown in Fig 4.10. During sputtering, argon gas is admitted to the chamber by a Mass Flow Controller at a flow rate of 10 sccm to maintain a pressure of 20 mTorr inside the chamber. A capacitance manometer, with a range 0-1 Torr, measures the pressure inside the chamber, which gives the input in the form of a voltage signal to a PID controller. The PID controller controls the position of a gate valve in front of the cryo pump. Depending on the increase or decrease in the argon pressure

inside the chamber, the PID controller opens or closes the gate valve. After deposition, the chamber is vented by flowing nitrogen through the vent valve.

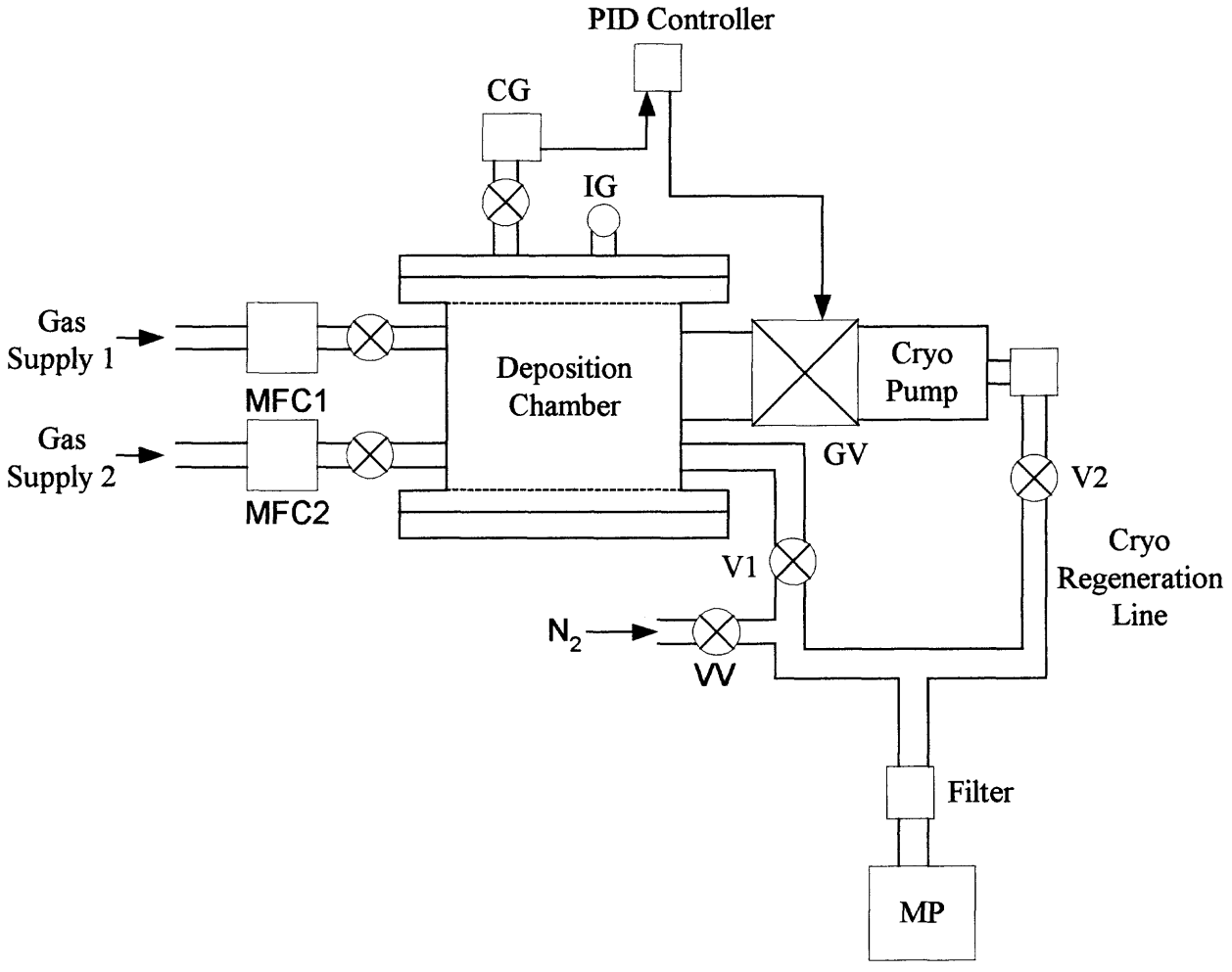

Fig 4.10 Schematic of vacuum and gas flow control of the deposition chamber

MFC - Mass Flow Controller
MP - Mechanical Pump
V1 and V2 - Valves
VV - Vent Valve
CG - Capacitance Gauge
IG - Ionization Gauge
GV - Gate Valve

4.4 Testing of the Chamber

The chamber is pumped by a mechanical pump to a base pressure of 100 mTorr in 10 min. and then by a cryo pump to a base pressure of $1.0x10^{-7}$ Torr. The base pressure obtained varies with the pumping time. With a 3-4 hours of pumping by cryopump the base pressure obtained is in the medium vacuum range with a value around $1.0x10^{-6}$ Torr. But when the chamber is pumped overnight the base pressure obtained is close to $1.0x10^{-7}$ Torr.

The values of the gas flow rate through the mass flow controller, for various stable pressures in the range of 5 – 60 mTorr and gate valve positions is shown in Table 4.1.

Table 4.1 Gas flow rates for various stable pressure conditions

Pressure (mTorr)	Gas flow rate (sccm)	% gate valve closed	Set point low	Set point high
5	10	79.5	4.6	5.4
10	10	80.8	9.6	10.4
20	10	81.0	19.6	20.4
30	8	81.0	29.6	30.4
40	11	81.6	39.6	40.4
50	11	82.4	49.6	50.4
60	11	83.2	59.6	60.4

The data in Table 4.1 shows that the pressure in the chamber is very sensitive to the gate valve position. The last two columns show the set range of the controller gauge for automatic pressure control. The difference between high and low set point determines the proportional band of the controller – a smaller difference controls the higher gain.

The initial analysis of the chamber with an RGA analyzer showed that the chamber was contaminated with water, nitrogen, hydrogen and other gaseous species. Oxygen content in the chamber was found negligible as a cryo pump effectively pumped

it. In order to remove these residual gases from the chamber, it was heated with three halogen bulbs upto a temperature of 120 °C from outside and pumped overnight with a cryopump. The chamber was baked in two steps one with a 1½ hr baking and the other one with 10½ hr baking. The results of the RGA for 1½ hr and 10½ hr are shown in Fig. 4.11 and Fig. 4.12 respectively.

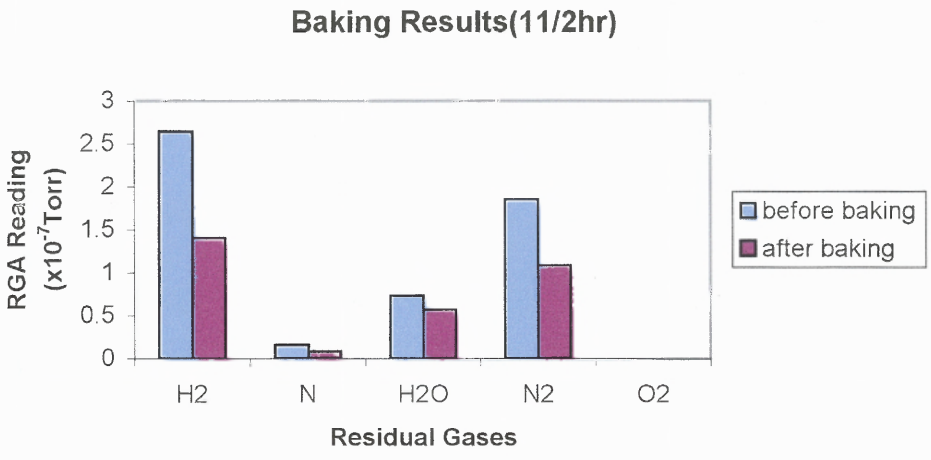

Fig 4.11 RGA analysis after 1½ hr baking

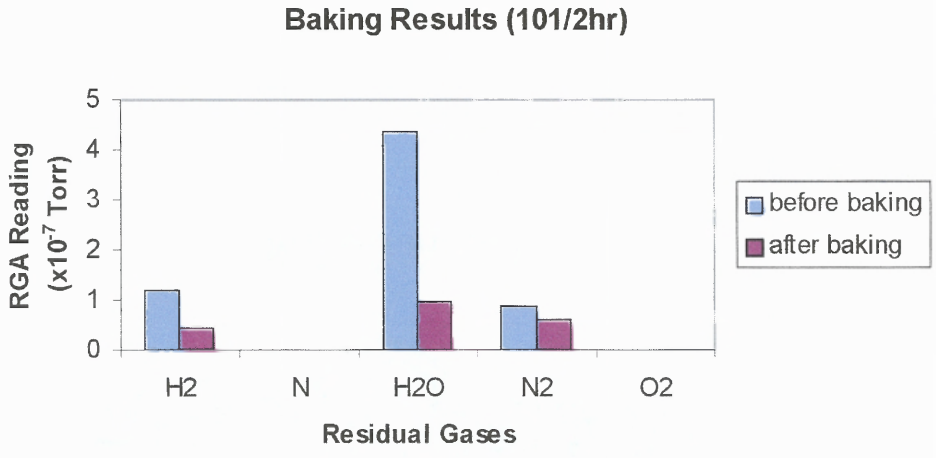

Fig 4.12 RGA analysis after 10½ hr baking

The charts shows that after 1½ hr baking a significant decrease in the content of water and a smaller decrease in nitrogen (N_2) and hydrogen was observed. But after 10½ hr baking a much larger decrease in the content of all gases was observed.

RGA reading were also taken before and after sputtering for 10min each. The results for the RGA for the first run are shown in Fig. 4.4 and Fig. 4.5 shows the results for the second run.

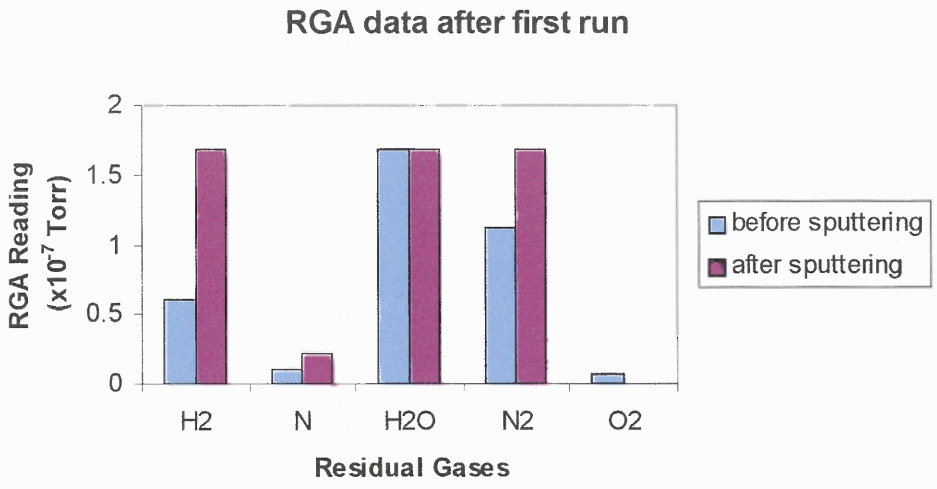

Fig 4.13 RGA reading for the first run of sputtering

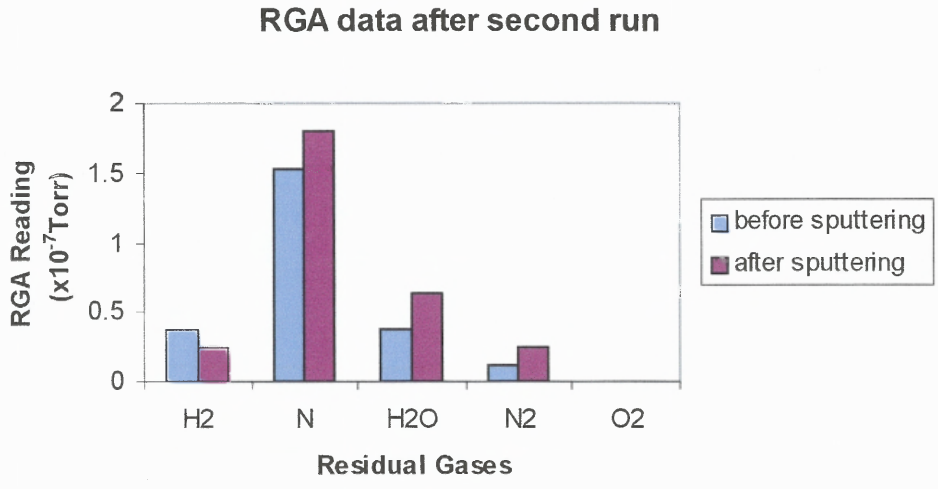

Fig 4.14 RGA reading for the second run of sputtering

Both after the first and second run of sputtering an increase in nitrogen, hydrogen and water content were observed. This may be due to the heating of the chamber while sputtering. Oxygen was absent after both the runs as it might have been gettered by the tantalum target which was observed red-hot after the power to the source was turned off.

4.5 Deposition of Tantalum

The tantalum target of 2" in diameter and 0.125" in thickness with 99.999% purity is mounted on a water-cooled torus magnetron-sputtering gun. Prior to deposition the target is sputter cleaned for ten minutes with the sample platter rotated to a position in which all substrates are shielded from the gun.

Deposition is usually carried out in the range 700 - 900 watts of power. The maximum power that can be supplied to the sputtering gun is limited to 1 kW. The power is supplied from a d.c. power supply which can operate in either voltage control or current control mode. Argon of 99.999% purity is used as the sputtering gas and is flown into the chamber through a mass flow controller at a flow rate of 10 sccm to maintain a constant pressure of 20 mTorr. The samples can be heated with a halogen bulb to a temperature of 300 °C prior to deposition.

The substrates used to deposit tantalum were of steel and silicon. The steel samples were polished with abrasive paper starting with 120 grit size upto 500 grit size in the order 120, 180, 240 and 500. The samples are finally uniformly polished with a finer lapping compound on a lapping plate. The steel samples were then cleaned in a bath of alconox (an industrial cleaning agent), acetone and propanol for 20 min each in an

ultrasonic cleaner, while the silicon samples were cleaned only by acetone and propanol in an ultrasonic cleaner.

After mounting the samples inside the chamber, the chamber is baked by three halogen bulbs upto 200 °C and pumped by a cryopump overnight to obtain a background pressure of $1.0x10^{-7}$ Torr. Prior to sputtering the samples are heated with a halogen bulb to a temperature in the range of 100 °C to 300 °C. Films are deposited at argon pressure of 20 mTorr and at a power of 900 Watts for 10min. A mass flow controller regulates the argon gas flow inside the chamber and gas is flown at a flow rate of 10 sccm.

After deposition the samples are allowed to cool in high vacuum. Venting of the chamber is done with pre-purified nitrogen gas (99.998% pure with O_2, CO, CO_2, THC, H_2O<10ppm) in order to avoid the oxidation of the samples.

CHAPTER 5

CYLINDRICAL DC MAGNETRON SPUTTERING SYSTEM

5.1 Operating Principle

A schematic diagram of the d.c. cylindrical magnetron system is shown in Fig 5.1.

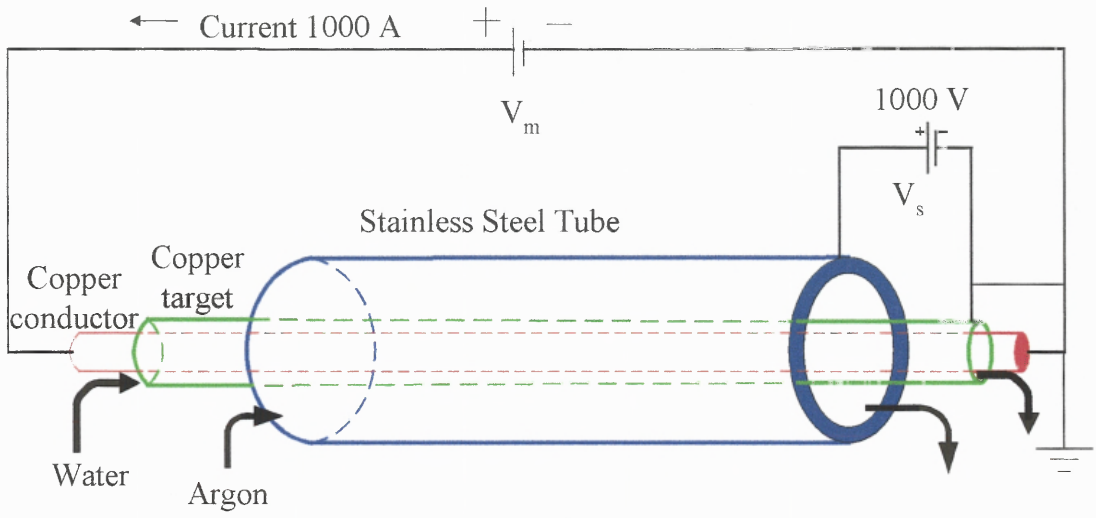

Fig 5.1 Substrate mounting and electrical circuit diagram

Its purpose is to carry out deposition on the inside surface of the steel tube. A cylindrical steel tube of 3.000" dia. was used as the substrate. In order to coat the inside surface of this tube a copper tube of 0.50" inside diameter and 0.625" outside diameter was used as a preliminary target for testing of the system. This target was concentric with the steel substrate tube. Since the steel tube shields outside magnetic field, the field for magnetron type sputtering was provided by passing a high dc current inside the target. A solid copper rod of 0.125" dia. was placed inside the target tube. A d.c. current in the range of 0-1400 Amps created the magnetic field. To generate a calculated magnetic

field of 314 Gauss on the surface of the target 1000 Amps current had to flow through the solid copper rod. Due to the copper rod resistance a power of 1.07 kW was dissipated in 1m length of the rod at 1000 Amps. Hence adequate cooling was required which was accomplished by flowing water between the target tube and the copper conductor. To create the plasma, argon gas at a pressure of 30 to 200 mTorr was admitted to the system and a voltage up to 1000 volts was applied between the steel tube and the copper target, with the target at ground potential.

5.2 Description of the System

The cylindrical sputtering system was designed and built at the Ion Beam and Thin Film Research Laboratory at NJIT. The vacuum enclosure of the system was built out of conflate™ components and ceramic insulators and, sealed with copper and viton o-rings. The total height and length of the system is 73" and 48" respectively. In the initial geometry the 2" or 3" diameter substrate tube was supported from inside by ceramic supports which were mounted on the target. The substrate was mounted inside the central section of the system supported with the help of an aluminum ring at both ends and contact with the stainless steel flange is made with a copper wire as shown in Fig. 5.2.

Argon gas pressure inside the chamber can be controlled manually by adjusting the position of the manual needle valve on the gas supply cylinder. A capacitance manometer (MKS Type 122A) monitors pressure during sputtering. The target inside the chamber is cooled with a water supply. The chamber is pumped by a mechanical pump to a base pressure of 2.0×10^{-3} Torr and then by a turbo molecular pump to a base pressure of 2.0×10^{-6} Torr. During deposition the power is supplied to the central flange to initialize the plasma inside the stainless steel substrate tube.

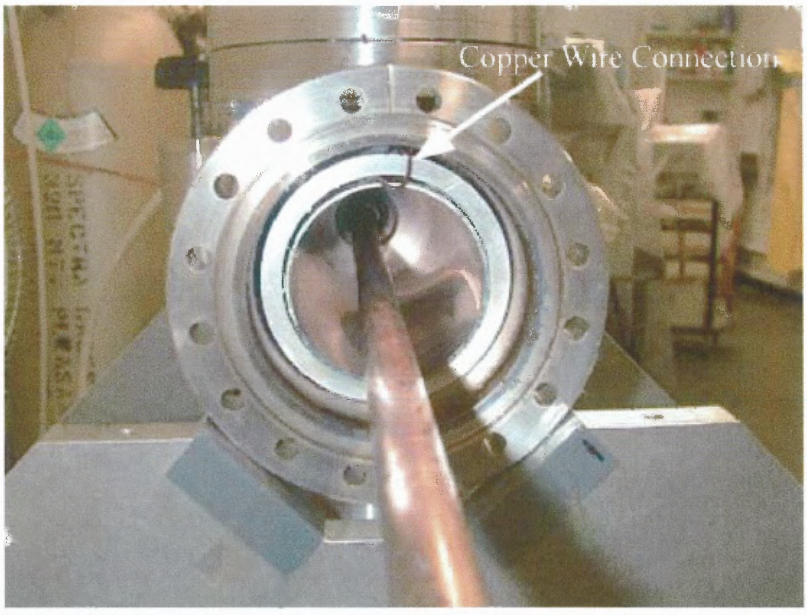

Fig 5.2 Substrate mounting inside the cylindrical chamber

This sputtering system had the major problem of plasma control and heating of the chamber walls upto temperatures like 200 °C in less than a minute during sputtering and it went through major changes in terms of geometry as shown in Fig 5.2, Fig 5.5 and Fig 5.7 and pumping as will be described in detail further in this chapter. The initial geometry of the system is shown in Fig. 5.3 and Fig. 5.4. Hence studies were carried out with a copper target, instead of a tantalum target, during the study of plasma control for economical reasons. In future with a proper plasma control and chamber heating, copper target will be replaced by tantalum target.

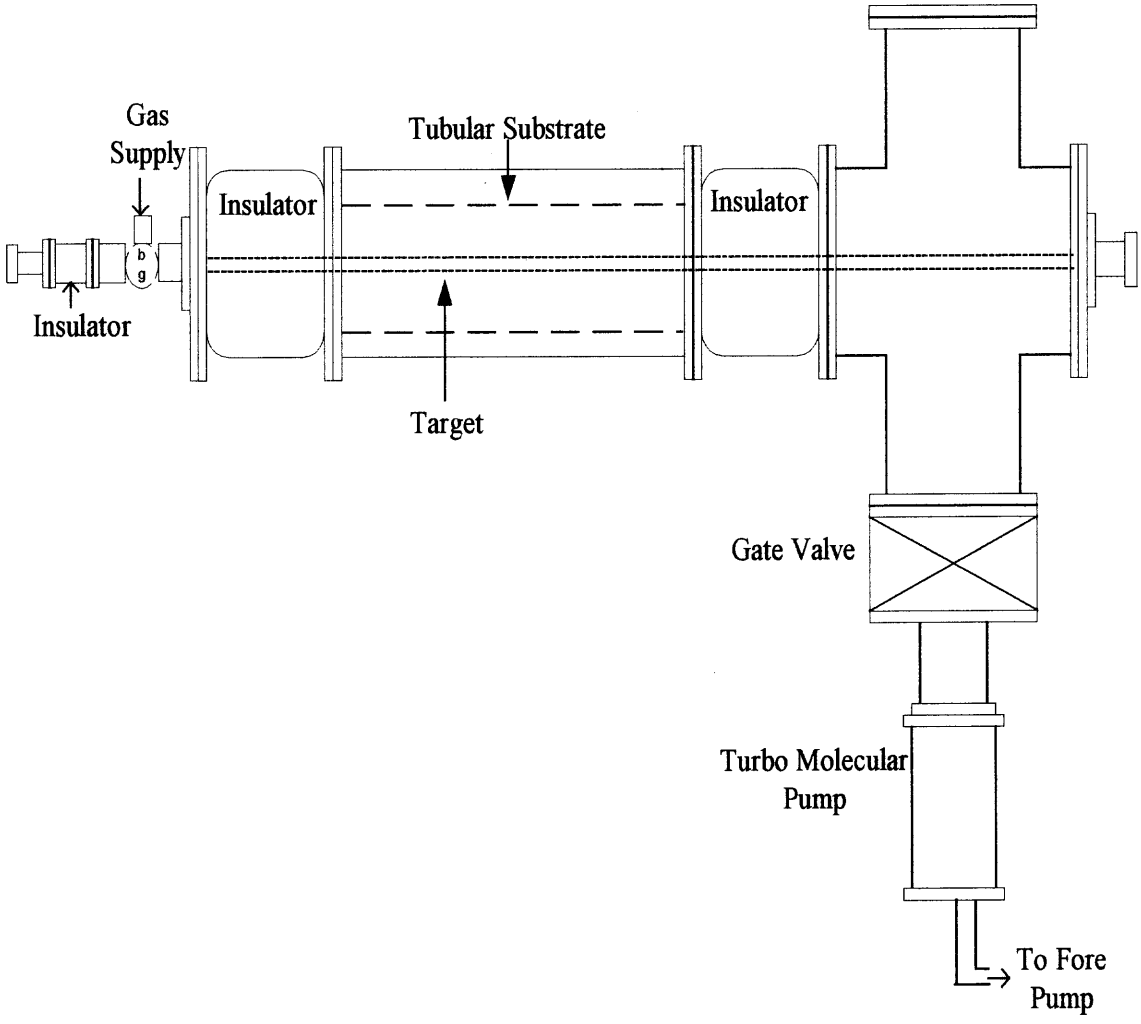

Fig 5.3 Initial geometry of the cylindrical system

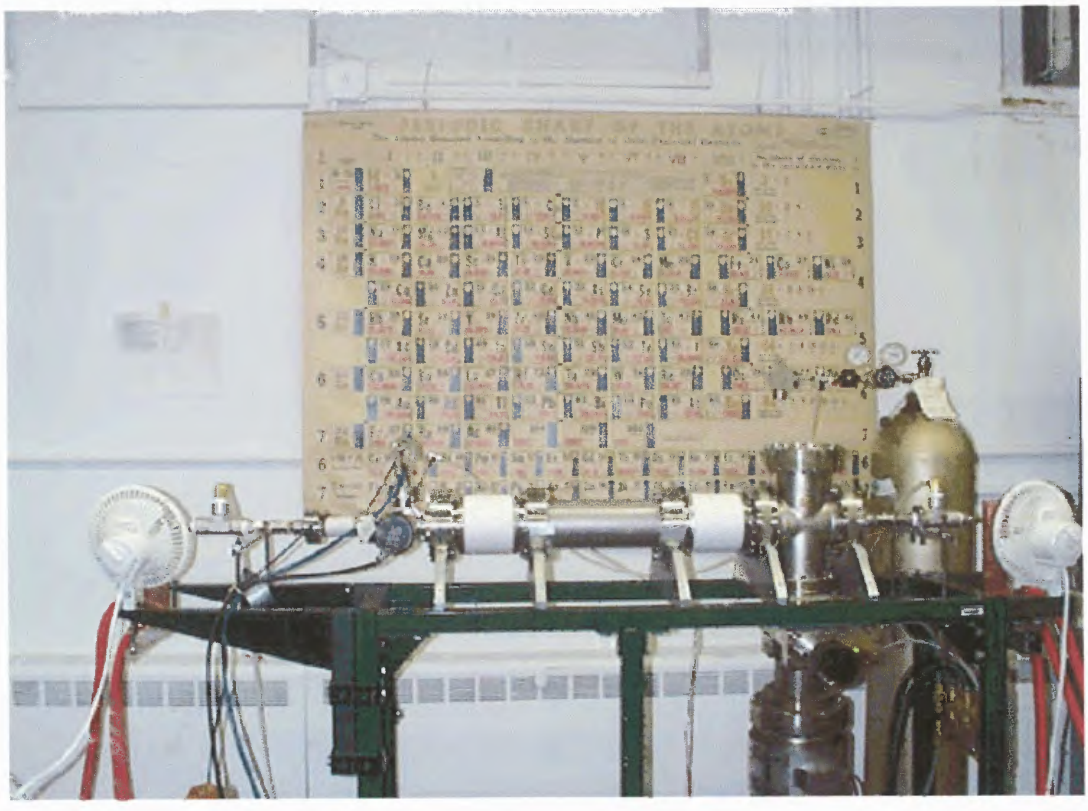

Fig 5.4 Initial cylindrical magnetron sputtering system

5.3 Plasma Control

The initial geometry of the system had a pumping port at one end while the gas was flown inside the chamber at the other end as shown in Fig 5.3. The central tube where the substrate was mounted was attached to 6.0" diameter insulators, to insulate the system from the high voltage applied to the central flange. This configuration gave the plasma a bigger geometry on both the sides of the central tube. It was observed that the plasma was flowing on the right hand side of the system easily in the 6" tube, as compared to the leftmost 2 ¾" tube. This was observed at both the polarities of the magnetic field on the either side of the system, and at argon pressures ranging from 30 mTorr to 200 mTorr. The plasma was heating up the right hand side flange to 200 °C in less than a minute. It was seen that this flange was getting sputtered and a thin coating of stainless steel was observed on the copper target.

It was noted that the ceramic insulators on the either side of the central tube were also getting coated with copper, so even at very low pressure of $1x10^{-5}$ Torr current was drawn from the power supply. In order to prevent the insulators from getting coated a glass tube was kept on the target on either side in the portion of the insulators. This helped in preventing the insulators from getting coated further.

Also here an attempt was made to keep a metallic ring on the top of the glass tube inside the insulator, touching the right hand side flange. It was thought that as the metallic ring is grounded with respect to the central flange, plasma will heat up the ring but would not proceed further ahead in the flange. But the ring was heated up heavily by the plasma and started melting.

The plasma was seen not flowing on the extreme left-hand side, as there was a 2 ¾" flange attached to the 6.0" insulator, which was reducing the volume. This led to the conclusion

1) to keep a smaller cross on the right hand side and
2) to shift the turbo pump at the center to create a symmetry in geometry with respect to pumping.

A 2 ¾" flange was kept on the right hand side and the pump was shifted in the middle as shown in Fig 5.5. Also the central tube was replaced with a 6" conflate cross.

When the plasma was initialized it was found that the smaller flanges on both side of the system were preventing the plasma to enter them even at very high pressure (>140 mTorr) and at alternative polarities of the magnetic power supply on either side of the system. But it was found that the plasma was heating the bellows kept below the central flange. Hence the bellows were shifted above the insulator. Now here as the bellow was in direct contact with the central flange, it was not getting heated up but the mechanical gate valve right below the ceramic insulator was getting heated up. This led to the conclusion that whatever was grounded from the central portion, where the high sputtering voltage is applied, was getting heated if the plasma is flowing in that portion and that's where the ions give up the energy.

The mechanical valve was replaced by a pneumatic gate valve and the ceramic insulator was taken away. An additional pumping hose was added and was connected to the right side 2 ¾" flange for pumping during sputtering. The gate valve was shifted at the top in contact with the central flange so that it is also at high voltage. The remaining of the chamber below the gate valve was grounded by small insulating brakes between the pneumatic valve and the stainless steel tube. It was assumed that as the gate valve is

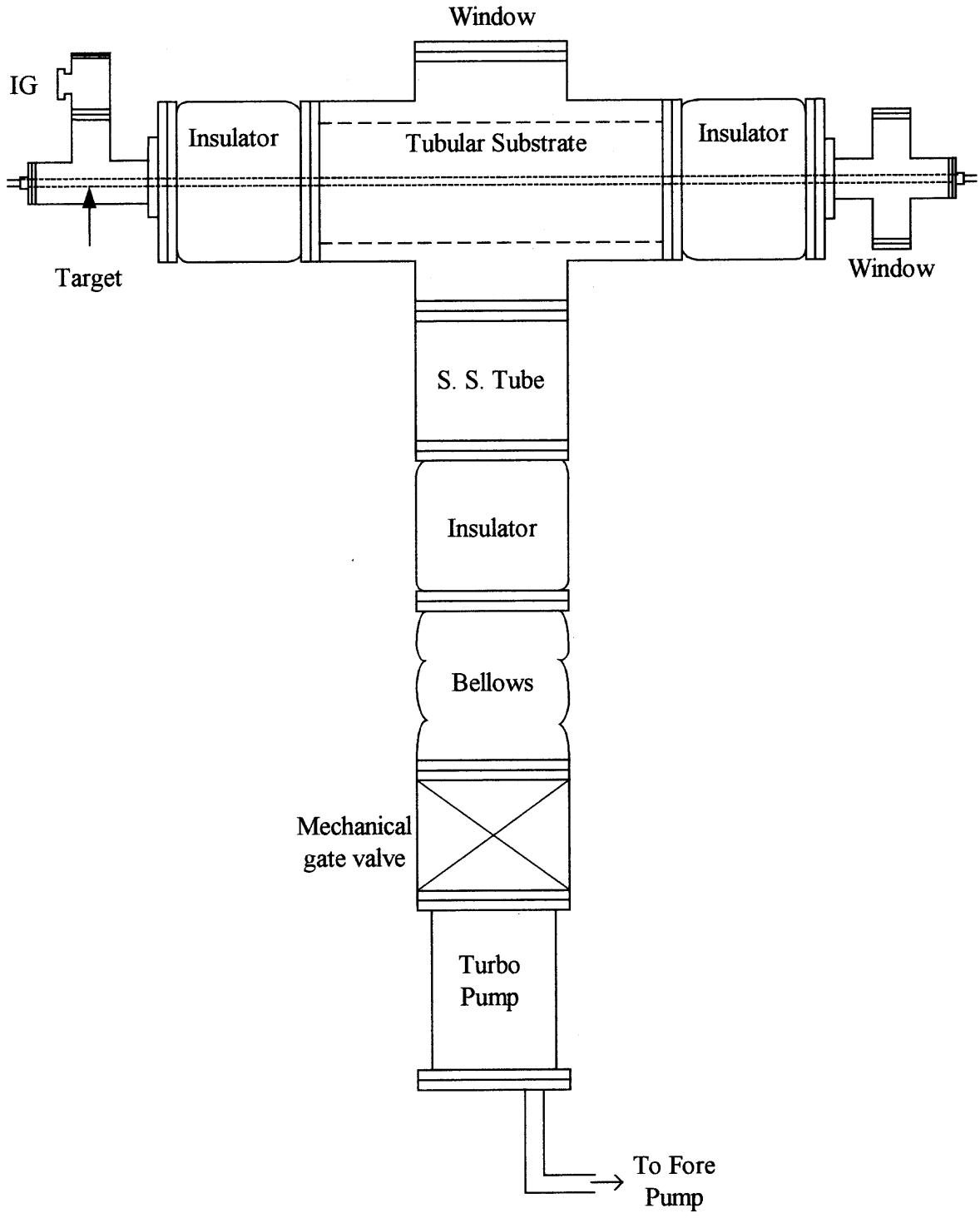

Fig 5.5 Intermediate geometry of the cylindrical system

in contact with the central flange the plasma would not travel into it and as the gate valve was kept closed during sputtering the plasma would not flow below it and would be restricted inside the central flange.

Other tests like removing the substrate and observing the plasma flow were performed. During these tests it was observed that the small diameter insulators with the 2 ¾" tubes at the two ends of the system where helping in preventing the plasma from flowing through them. So it was decided to replace one of the 6" insulator with 2 ¾" insulator on the left-hand side and try the plasma flow. With this configuration it was observed that the plasma was not flowing into the 2 ¾" insulator on the left-hand side but was flowing easily into the 6" insulator on the right-hand side and was restricted by the 2 ¾" tube further ahead. The plasma flow was tried by switching the magnetic field polarities at both the ends of the system alternatively, but it was seen to be restricted by the reduced geometry on the left-hand side. Plasma spreads in a chamber, because it is positive with respect to the chamber wall so ions are accelerated to the wall. But the 2 ¾" insulator might be getting charged up and counteracting this potential difference.

So the 6" insulator on the right hand side was also replaced by a 2 ¾" insulator and plasma flow was tried. It was observed that the plasma was now restricted inside the central flange. But now this configuration poses an additional problem of pumping the chamber as the chamber volume is reduced on either side of the central flange. Efforts are on to solve this problem.

Once the problem of pumping is solved with this final configuration of the system copper target would be replaced with a tantalum target and studies would be carried out on the tantalum films obtained with this system.

Fig 5.6 Final cylindrical magnetron sputtering system

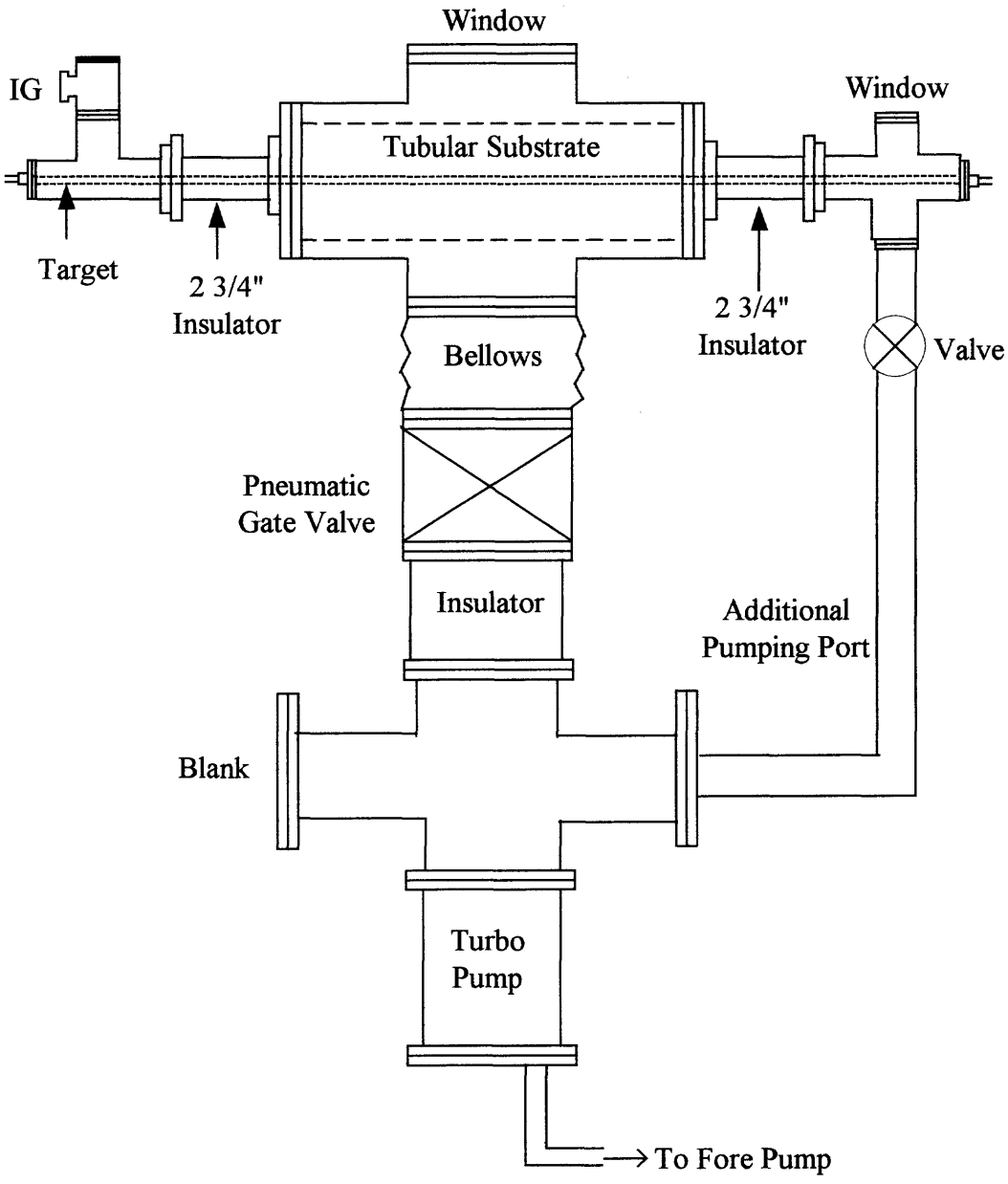

Fig 5.7 Final geometry of cylindrical sputtering system

The sputtering voltages vs. the magnetizing current characteristics for the initial stable plasma conditions are shown in Fig. 5.8. The magnetizing current helps in creating magnetic field, which keeps the electrons confined to the plasma and reducing loss to the chamber walls as described in section 3.3. The curve shows that a very limited range of

VI conditions exists for a pressure of 30 mTorr indicating that the plasma is not stable below 30 mTorr. At a sputtering voltage below about 520 V the plasma extinguishes. But

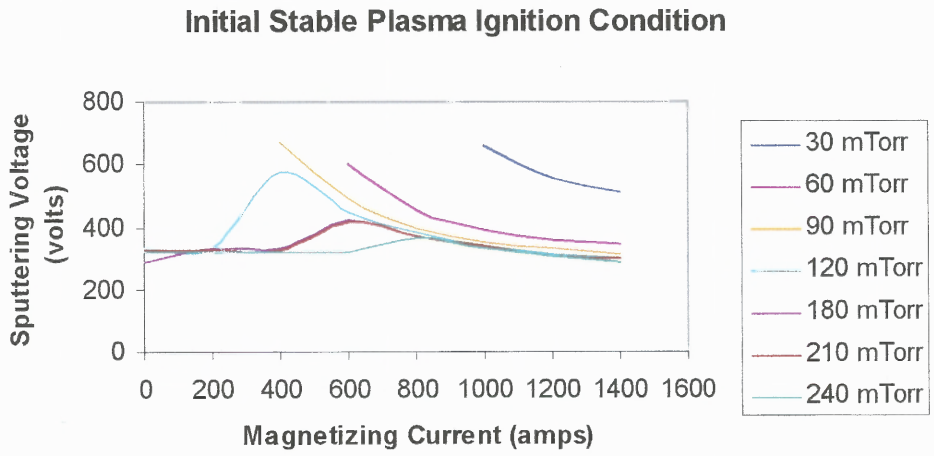

the range is widened for higher pressure.

Fig 5.8 Initial stable plasma ignition condition

CHAPTER 6

TANTALUM FILM ANALYSIS

6.1 Introduction

This chapter discusses the result of tantalum film analysis by various methods, which include:

1) Dektak Film Thickness Measurement
2) Scanning Electron Microscopy
3) X - Ray Diffraction Technique
4) Rutherford Back Scattering

6.2 Measurement of Film Thickness

The thickness of tantalum film deposited on silicon was measured with a Sloan Dektak II film thickness measurement unit with a resolution of 0.1 μm. It works by gently dragging a mechanical stylus across a surface. Its output is a graph of stylus height vs. position, from which step height, surface roughness, and other features can be determined. Profiles of the surface step were measured at the film edge. The step was formed because the screws holding the sample masked a part of the substrate. Examples of the step profile are shown in the following Fig 6.1 and 6.2.

The thickness of the film shown in Fig. 6.1 is 6100 Å. The film was deposited at 20 mTorr pressure with 918 W of power for 15 min. The thickness of the film shown in Fig. 6.2 is 4490 Å. This film was deposited at a pressure of 20 mTorr with a power of 875 W for 10 min. The films discussed in this thesis ranged from 4000 Å to 6000 Å.

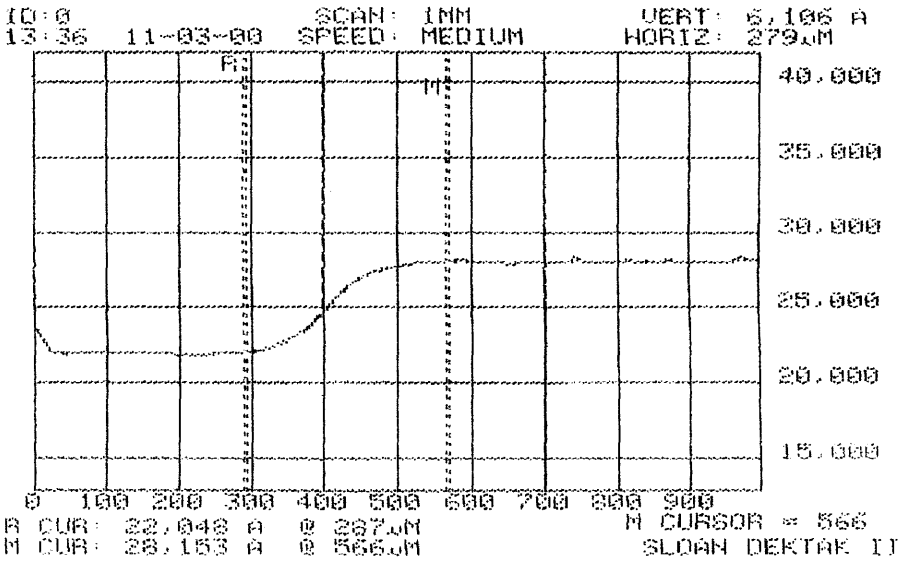

Fig 6.1 Dektak profile for tantalum film deposited on silicon – film thickness 6100 Å

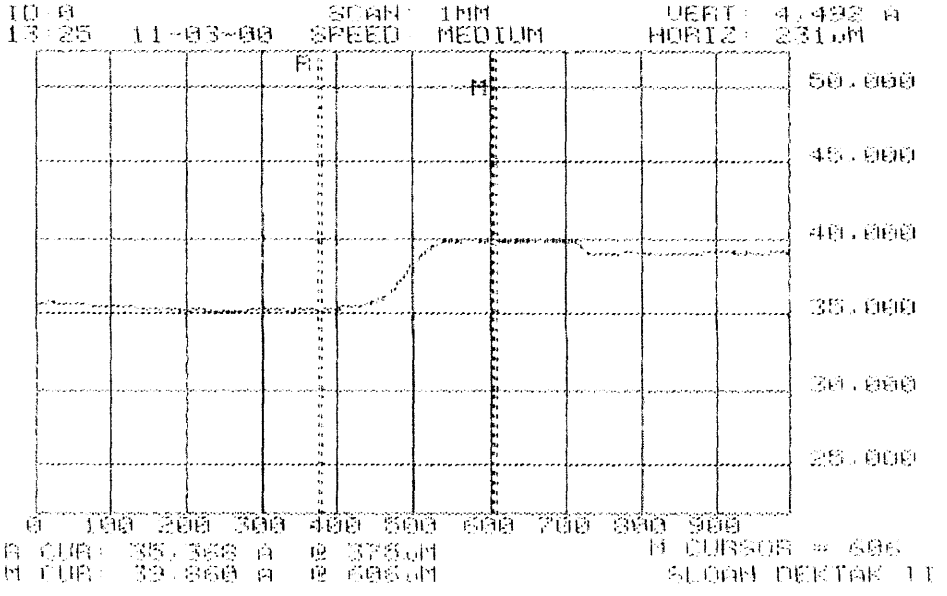

Fig 6.2 Dektak profile for tantalum film deposited on silicon – film thickness 4490 Å

6.3 Scanning Electron Microscopy

A Scanning Electron Microscope consists of an electron accelerator that focuses the electron beam from a tungsten filament on to the specimen with the help of electromagnetic lenses and a detection system measuring the intensity of electrons scattered by the specimen. An image is formed by raster scanning the beam on the specimen [31]. SEM images of various films were taken with an Environmental Scanning Electron Microscope from Electroscan. They included tantalum films deposited on steel and silicon under various conditions of substrate surface cleaning, substrate surface treatment prior to deposition and substrate surface polishing.

As an example in one of the observations it was noted that when a steel substrate was polished with a dico brand emery heavy cut buffing compound the tantalum films deposited on that substrate showed the pattern corresponding to the polish lines present on the steel substrate, as shown in Fig 6.9. The pattern is different from the conformal coverage of the fine – polished steel shown in Fig. 6.5 and 6.6.

In one more observation it was seen that flaky and non continuous film of tantalum on steel substrate was obtained as shown in Fig 6.3, when it was cleaned only with acetone.

Hence a proper cleaning and polishing procedure was developed to clean and polish the substrates prior to deposition. The steel substrates were then cleaned and polished as described in section 4.5.

The substrate surface condition can also be effected by treatment in the deposition chamber, prior to film deposition. In some cases, rough and non-uniform

films were observed on steel samples when they were not pre-heated prior to deposition, despite proper cleaning and polishing of the substrate surface. An example is shown in Fig 6.4.

But when another set of steel substrates were heated to 300 °C with a halogen bulb during the same run prior to deposition, the films observed were smooth and adherent to the substrate. An example is shown in Fig 6.5.

Hence the substrates were properly cleaned, polished and heated for the films deposited after this observation. The films obtained were smooth and continuous. Two examples are shown in Fig 6.5 and Fig. 6.6. This showed that substrate surface condition plays an important role on the quality of films deposited. Fine lines visible on the surface of the films in Fig. 6.5 and Fig. 6.6 are due to conformal coverage of polishing lines seen also on the substrate prior to deposition. A different pattern on the surface was observed with a rougher polishing and without any pre-heating of the sample. The dark irregular surface features appear to be aligned with the polishing direction but are not continuous. They may have different crystalline phase composition than the lighter areas.

The difference in the appearance of smooth films (on polished substrates) which are predominantly of either alpha or beta phase is seen under high magnification (Fig. 6.7 and Fig. 6.8). The surface of beta phase film looks more grainy and has a pattern of fine cracks. Hieber and Mayer also observed such cracks in beta phase tantalum films deposited on Corning 7059-glass [29].

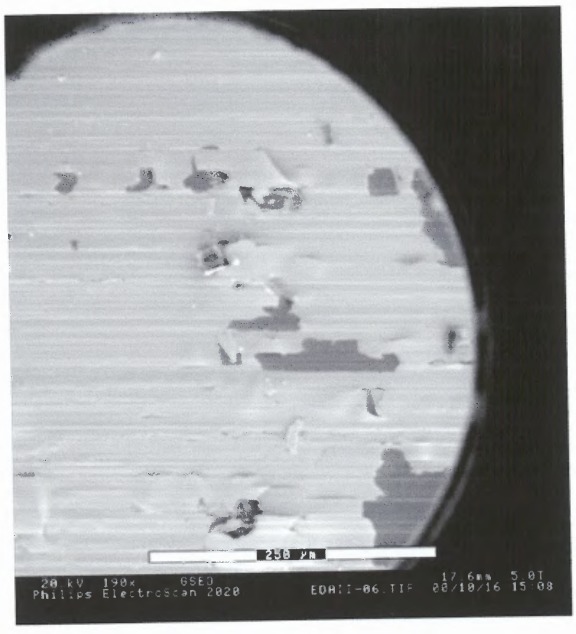

Fig 6.3 SEM image (190X) showing flaky tantalum films on steel substrate – film thickness 4000 Å

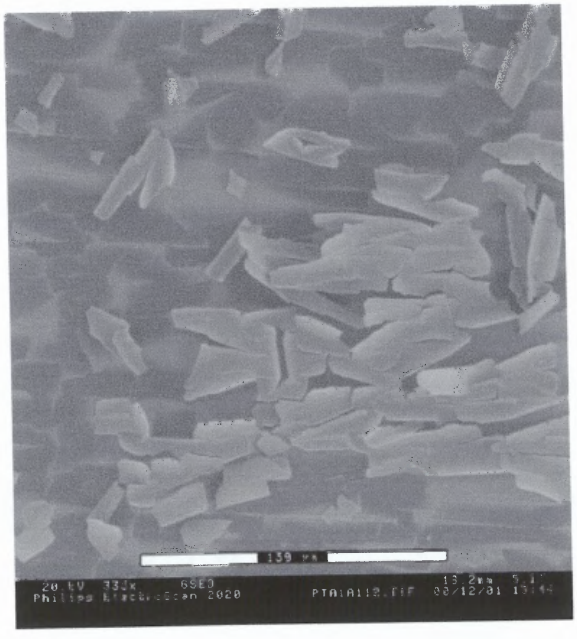

Fig. 6.4 SEM image (335X) showing rough and non-uniform film of tantalum on steel substrate without prior heating – film thickness 4000 Å

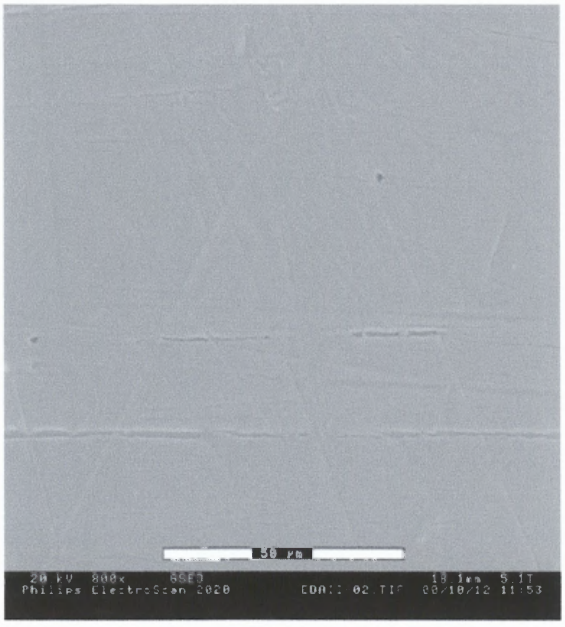

Fig 6.5 SEM image (800X) showing smooth film of tantalum on steel substrate after proper cleaning, polishing and heating – film thickness 4000 Å

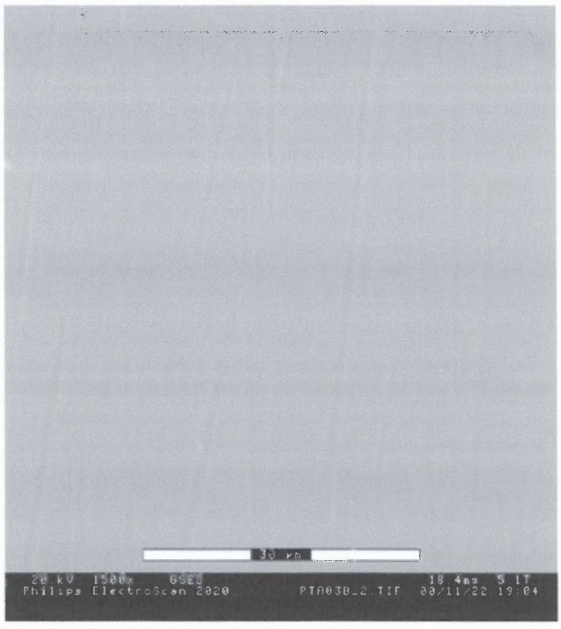

Fig 6.6 SEM image (1500X) showing smooth films of tantalum on steel substrate after proper cleaning, polishing and heating – film thickness 4000 Å

Fig 6.7 SEM image (360X) showing tantalum films deposited along polish lines present on steel surface – film thickness 6000 Å

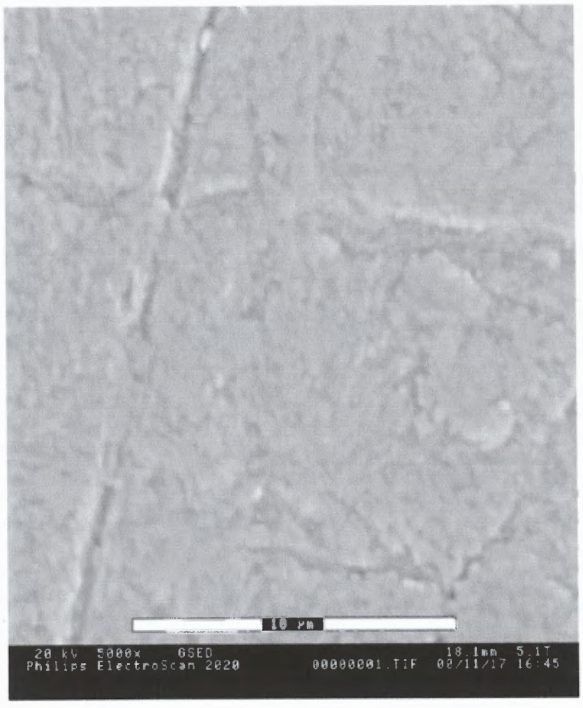

Fig 6.8 SEM image (5000 X) of beta tantalum on steel

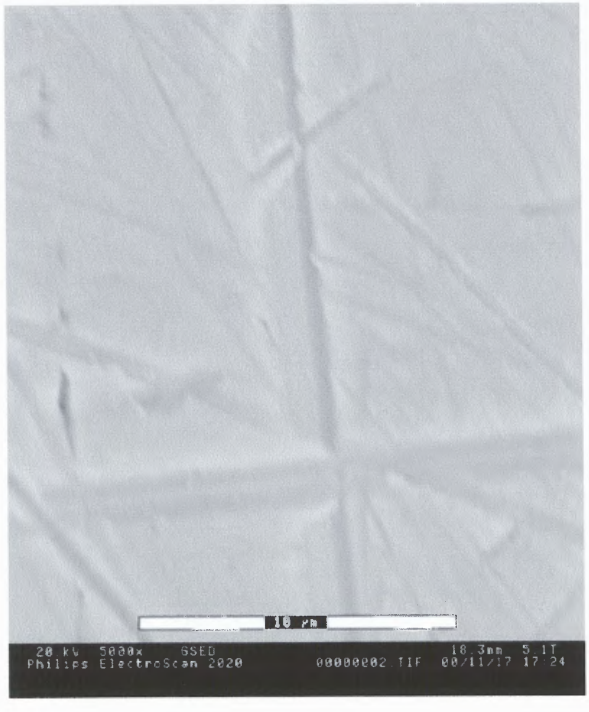

Fig 6.9 SEM image (5000X) of alpha tantalum on silicon

6.4 X - Ray Analysis

X-ray analysis of the films deposited was done using Philips Expert MPD instrument with Cu Kα radiation. The standard peaks for alpha tantalum and beta tantalum are shown in Fig. 6.10 and Fig. 6.11. These plots were taken from JCPDS - International Center for Diffraction Data (ICDD) PCPDFWIN v. 2.01. no. 04-0788 for alpha tantalum and no. 25-1280 for beta tantalum, 1998. They refer to powder samples in which grains are randomly oriented. In case of thin films a degree of alignment of the crystalline grains with respect to the substrate surface is expected. The alignment may significantly change 2-theta diffraction spectra, as the relative intensity of various lines may be very different than for the powder case.

XRD spectra of films obtained on a steel substrate and a silicon substrate is shown in Fig. 6.12 and 6.13 respectively. The samples were prepared under the same conditions. Sputtering was carried out for 10 min. at a power of 780 W and at 20 mTorr pressure with an argon flow rate of 10 sccm. Prior to sputtering the chamber was baked for 10½ hr and was pumped to 1.0×10^{-7} Torr base pressure.

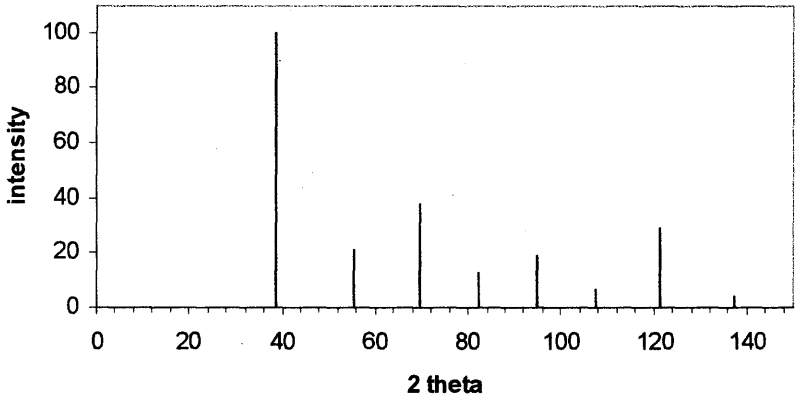

Fig 6.10 Standard diffraction lines for alpha tantalum

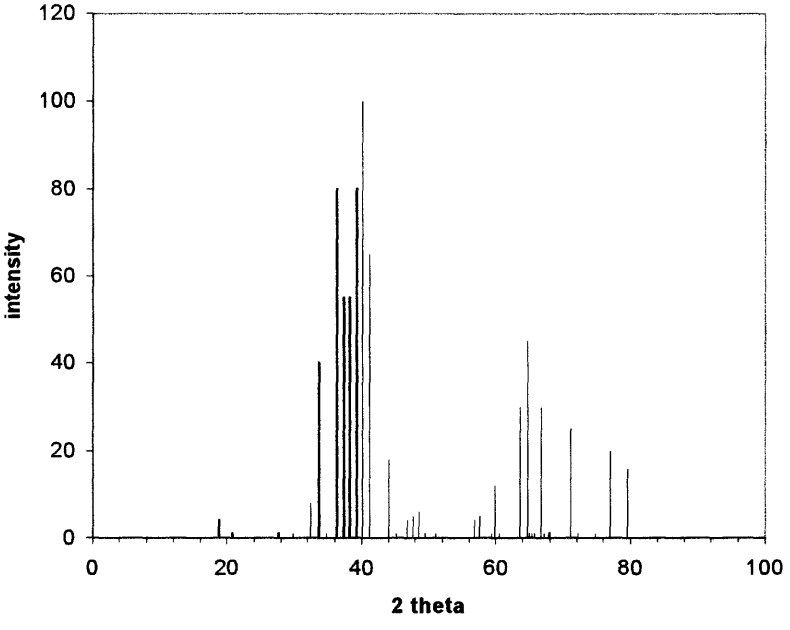

Fig 6.11 Standard diffraction lines for beta tantalum

Fig. 6.12 shows the presence of beta tantalum on steel with a corresponding Miller Indices of (202), (333) and (641) at 2θ = 38.200, 2θ = 65.339 and 2θ = 68.594 respectively. Read and Hensler [13] obtained same type of peak for tantalum films sputtered on glass substrates using the d.c. diode sputtering technique. The presence of beta tantalum is also confirmed when this plot is compared with the standard chart for beta tantalum, which shows a peak at 2θ = 38.2 and 66.708 with Indices (202) and (720) respectively. The fact that not all peaks of beta tantalum are seen in Fig. 6.12 may be explained by orientation of the film grown with respect to the substrate surface. The same reason can be given for absence of other major peaks for alpha tantalum at 2θ = 55.549, 69.581 and 121.349. The SEM image for beta tantalum is shown in Fig 6.8.

Fig. 6.13 shows the presence of alpha tantalum on silicon with a corresponding Miller Indices of (110) at 2θ = 38.472. Same peak was observed by Read and Hensler [13] for tantalum films sputtered on glass substrates using the d.c. diode sputtering technique with Miller Indices (110) and d = 2.35 °A. Lee and Windover [33] also observed the same peak for tantalum films sputtered on inner side of a steel tube covered with thin niobium layer using the triode sputtering technique. Sato has also observed the same peak for tantalum films deposited on aluminum film on SiC substrate [19]. This peak (2θ = 38.472) can be erroneously identified as the (202) beta-Ta as (2θ = 38.2) both the peaks are very close with a very small 2θ-difference [13]. The SEM image for alpha tantalum is shown in Fig 6.9.

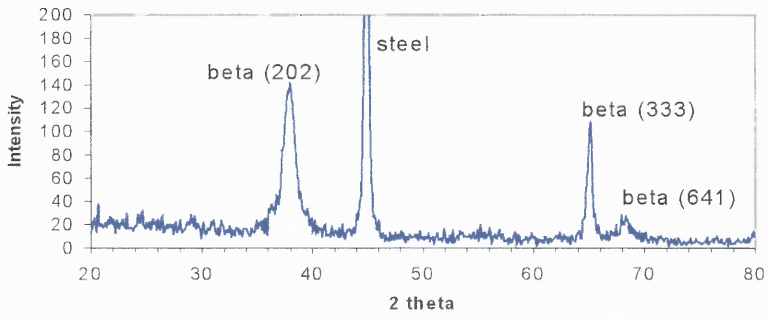

Fig 6.12 X-ray analysis of tantalum film showing peaks for beta tantalum

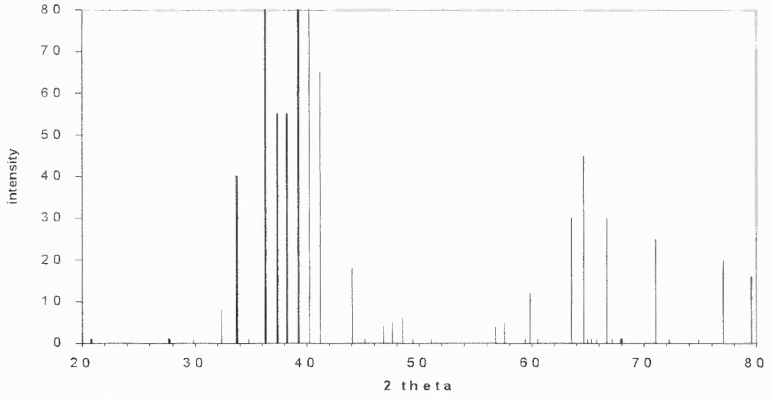

Fig 6.13 Standard diffraction lines for beta tantalum between 2θ = 20 and 2θ = 80

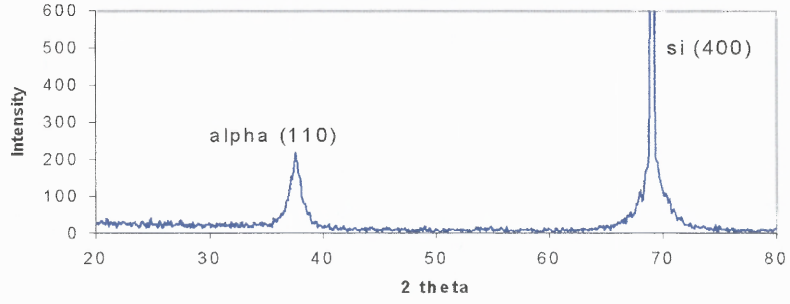

Fig 6.14 X-ray analysis of tantalum film showing peak for alpha tantalum

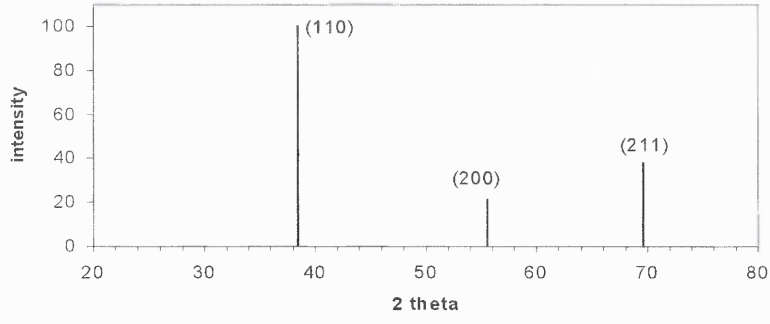

Fig 6.15 Standard diffraction lines for alpha tantalum between 2θ = 20 and 2θ = 80

Also in some cases a mixture of beta and alpha tantalum films was obtained for films prepared on steel substrates. These films were sputtered for 10 min. at 20 mTorr pressure and at a power of 825 W. Prior to sputtering the chamber was baked for 10½ hr and was pumped to $1.0x10^{-7}$ Torr base pressure. Two examples are shown in Fig. 6.16 and 6.17 respectively.

Fig. 6.16 shows the peak for beta tantalum at 2θ = 33.692 (002), 2θ = 65.339 (333) and 2θ = 71.028 (513) and for alpha tantalum at 2θ = 38.472 (110) and 2θ = 55.81 (200). Fig. 6.17 shows the peak for beta tantalum at 2θ = 33.692 (002), 2θ = 66.708 (720) and 2θ = 71.028 (513). It also shows peaks for alpha tantalum at 2θ = 38.472 (110), 2θ = 82.461 (220) and 2θ = 121.349 (321).

Table 6.1 Summary of XRD results

Standard Dominant XRD Lines		Observed XRD Lines			
α	β	Sample A	Sample B	Sample C	Sample D
	33.692	No	No	Yes	Yes
	38.200	Yes	No	No	No
38.472		No	Yes	No	Yes
55.810		No	No	Yes	No
	65.339	Yes	No	Yes	Yes
	66.708	No	No	No	Yes
	68.594	Yes	No	No	No
	71.028	No	No	Yes	Yes
82.461		No	No	No	Yes
121.349		No	No	No	Yes

Sample A – Fig. 6.12 Sample B – Fig. 6.13

Sample C – Fig. 6.16 Sample D – Fig. 6.17

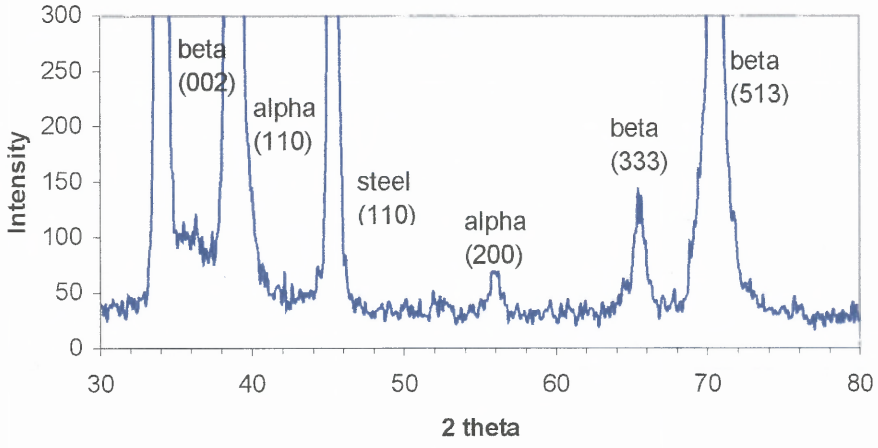

Fig 6.16 X-ray analysis of tantalum film showing peak for alpha and beta tantalum

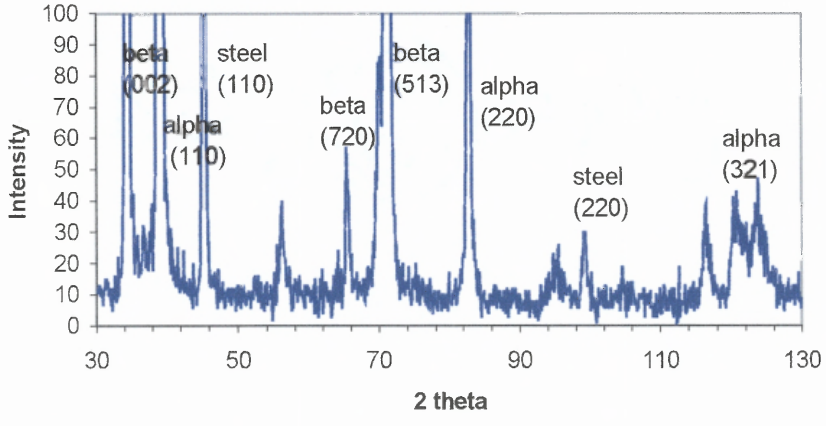

Fig 6.17 X-ray analysis of tantalum film showing peak for alpha and beta tantalum

(Steel 110 peak and 220 peak correspond to 110 peak and 220 peak of Fe, respectively.)

6.5 Rutherford Back Scattering

RBS measurement with 2 MeV He^+ beam were made on selected samples using National Electrostatics Tandem Accelerator at Bell Laboratories, Murray Hill, NJ and Army Research Laboratory, Aberdeen, Maryland. To facilitate the analysis, tantalum films were deposited on silicon substrates, which were usually mounted for this purpose on the same sample holder with steel substrates. Fig. 6.18 shows the RBS spectrum for a sample deposited with 900 W of power at a pressure of 20 mTorr for 10 min. The sample was deposited without baking of the chamber or substrate preheating. Analysis of the data by comparison of the measured spectrum with a simulation done with a RUMP program (Computer Graphics Service Ltd. v. 4.00 [beta], 1999), which is also shown in Fig. 6.18, indicates that film contains 50% tantalum. The remaining 50% of the film is most likely to be oxygen. Precise determination of the oxygen content is difficult because oxygen peak in the spectrum is masked by a much intensive silicon signal.

Fig 6.19 shows the RBS plot for samples, which were heated, to 300 °C prior to deposition. These samples were deposited with a power of 900 W at 20 mTorr pressure for 5 min. Also prior to deposition the chamber was baked for 10½ hr. and was pumped with a cryopump to a base pressure of 1.0×10^{-7} Torr. The RGA results after baking of the chamber for 10½ hr. are shown in Fig. 4.12. Simulation done with a RUMP program, which is also shown in Fig. 6.19, indicates that the film consists of 100% tantalum.

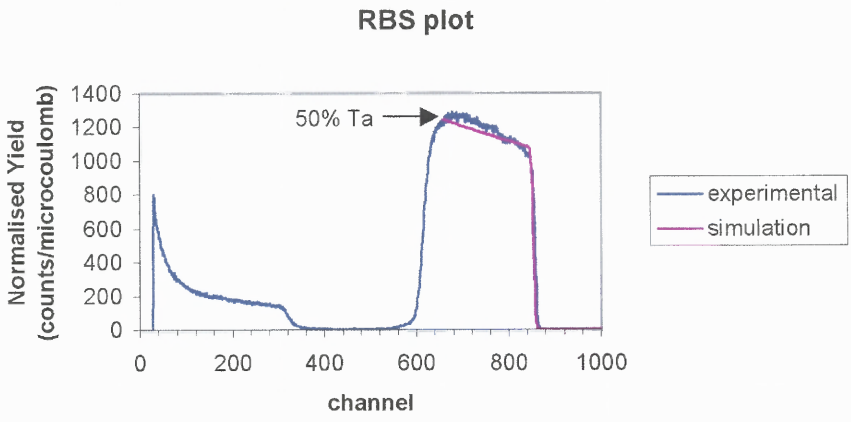

Fig 6.18 RBS plot of tantalum films deposited on silicon without baking of the chamber and substrate pre-heating

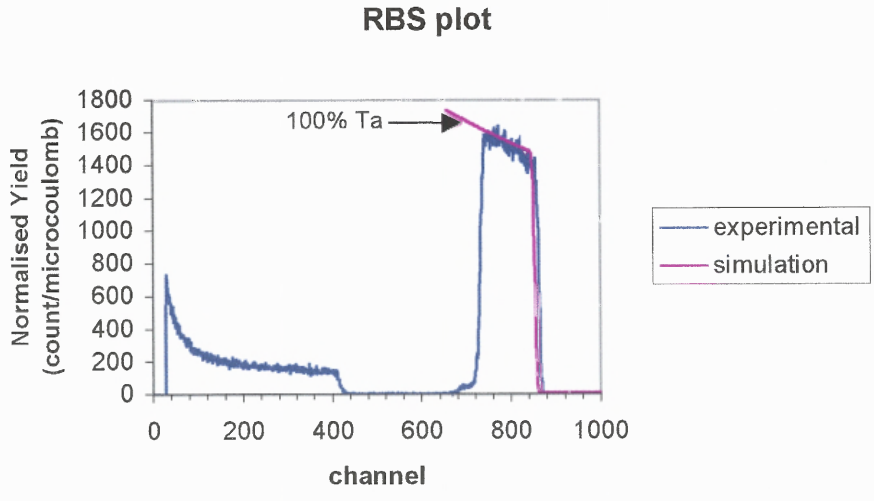

Fig 6.19 RBS plot for tantalum films deposited on silicon after baking of the chamber and substrate pre-heating

CHAPTER 7

SUMMARY AND CONCLUSIONS

The results of this thesis are summarized in the following sections.

7.1 Testing and Development of Deposition Equipment

7.1.1 Planar D. C. Magnetron Sputtering System

Vacuum and gas flow control system consisting of a cryogenic pump, mechanical pump, controlled gate valve and mass flow controller was tested. The base vacuum achieved in the chamber was 1.0×10^{-7} Torr. The regulation of gas pressure inside the deposition chamber was automated with a PID controller. A planar d.c. magnetron sputtering source with 2" diameter target was tested for sputtering of tantalum on steel and silicon. A, substrate platter accommodating up to 8 substrate holders was designed and built.

7.1.2 Testing of Cylindrical D. C. Magnetron Sputtering System

A cylindrical d.c. magnetron sputtering system was tested for vacuum, gas flow and plasma control. The system was redesigned during the process of testing to its current geometry. Stable operation was easily achieved with the reverse biasing, when the tubular substrate was negatively biased with respect to the grounded target and the vacuum enclosure. In normal biasing stable discharge could not be maintained with any magnetizing current up to 1400 A. Sputtering was possible only after installing of a special power supply with fast current control circuitry. During this operation plasma has

the tendency to propagate throughout the system from the positively biased substrate. The problem was partially solved by restricting the space between the target and insulating section of the vacuum enclosure. Other solutions will be tested in future work.

7.2 Tantalum Deposition

As part of a pilot study tantalum films were deposited on steel and silicon substrates and analyzed using profilometry, SEM, RBS and XRD techniques.

1. Thickness of tantalum films deposited on silicon and steel substrate was measured by a profilometer at the film edge between 4000 °A to 6000 °A.
2. Deposition rate at the source power of 900 W and 20 mTorr pressure is found to be 400 °A/min.
3. Integrity, appearance and adherence of the films were sharply influenced by the substrate type, substrate preparation and condition in the chamber.

   - Cleaning:

   It was found that proper cleaning of the steel substrates was essential for obtaining smooth and adherent films.

   - Polishing of the surface:

     Degree of polishing influenced the appearance of SEM of the film surface. Conformal coverage of polishing marks was visible on the surface of films on highly polished steel substrates. A more complex pattern of light and dark areas on rougher tantalum surface, aligned with unidirectional polishing pattern on steel surface pattern was seen. The image was suggestive of the presence of different tantalum phases.

- Substrate preheating:

Heating of substrates prior to deposition to 300 °C had a substantial influence on the quality of films produced. The preheating process can be considered as the last step in substrate cleaning, which desorbs gases, particularly water vapor, from the surface. Films, which were produced without pre-heating of the substrate, were often found to be poorly adhering and discontinuous.

4. Film composition

The composition of the films produced was highly influenced by the amount of residual gases present in the chamber. An RGA analysis showed a significant decrease in the amount of water vapor and oxygen in the residual gas after baking the chamber for several hours, when the chamber walls reached 110 °C. RBS analysis showed a high oxygen content (up to 50%) of the tantalum films deposited without proper substrate and chamber preparation. Close to 100% of tantalum content was found in the films deposited after proper chamber and substrate baking.

5. Crystallinity

XRD analysis of the deposited tantalum films showed the presence of both alpha and beta tantalum phases. The relative intensity of the alpha and beta peaks in the spectrum depended on the heating of the substrate. Heating of the substrate prior to deposition helped in increasing the amount of alpha tantalum, which requires further investigation.

REFERENCES

1. D. Mills, "The Structure of Sputtered Tantalum", J. of Can. Ceram. Soci., vol. 35, pp. 48-52, 1966.

2. P. N. Baker, "Preparation and Properties of Tantalum Thin Films", Thin Solid Films, vol., 14, pp. 3-25, 1972.

3. S. Wolf and R. N. Tauber, *Silicon Processing for the VLSI Era Vol. 1 – Process Technology*, Lattice Press, Sunset Beach, CA, 2000.

4. Karen Holloway and Peter M. Fryer, "Tantalum as a Diffusion Barrier Between Copper and Silicon", Appl. Phys. Lett., vol. 57, pp. 1736-1738, 1990.

5. W. D. Westwood, N. Waterhouse and P. S. Wilcox, *Tantalum Thin Films*, Academic Press Inc., NY, 1975.

6. Shivramkrishnan Prabha, "Characterization of Tantalum Coatings on Steel Substrates", *Master's Thesis, January 1999*, Materials Science and Engineering, New Jersey Institute of Technology, Newark, NJ 07102.

7. Sung Min Maeng, "Characterization of Steel Corrosion in an Aggressive Environment", *Master's Thesis, August 1999*, Dept. of Civil and Environmental Engineering, New Jersey Institute of Technology, Newark, NJ 07102.

8. J. F. Cox and E. D. McClanahan, "High Rate Sputtering of Tantalum onto Gun Steel", Benet Weapons Laboratory, Watervliet, NY, 1982 (requires special permission to get a copy).

9. D. W. Matson, M. D. Merz and E. D. McClanahan, "High Rate Sputter Deposition of Wear Resistant Tantalum Coatings", J. Vac. Sci. Techno., vol. 10, no. 4, pp. 1791-1796, 1992.

10. URL http://chemlab.pc.maricopa.edu/periodic/periodic.html (Oct. 30, 2000).

11. Webelement URL
    http://www.webelements.com/webelements/elements/text/Ta/key.html
    (Sept. 19, 2000).

12. L. A. Clevenger, A. Mutscheller, J. M. E. Harper, C. Cabral Jr. and K . Barmak, "The Relationship Between Deposition Conditions, the Beta to Alpha Phase Transformation, and Stress Relaxation in Thin Film", J. Appl. Phys., vol. 72, no. 10, pp. 4918-4924, 1992.

REFERENCES
(Continued)

13. Mildred H. Read and D. H. Hensler, "X-ray Analysis of Sputtered Films of Beta Tantalum and Body Centered Cubic Tantalum", Thin Solid Films, vol. 10, pp. 123-125, 1972.

14. M. H. Read and Carl Altman, "A New Structure in Tantalum Thin Films", Appl. Phys. Letters, vol. 7, no. 3, pp. 51-52, 1965.

15. W. D. Westwood and F. C. Livermore, "Radio Frequency Sputtered Tantalum Thin Films Deposited in an Oxygen Doped Atmosphere", Thin Solid Films, vol. 8, no. 1, R1-R2, 1971.

16. M. Croset and G. Velasco, "Structure and Composition of Sputtered Tantalum Films on Silicon Studied by Nuclear and X-ray Analysis", J. Appl. Phys., vol. 43, pp. 1444-1447, 1972.

17. L. G. Feinstein and R. D. Huttemann, "Factors Controlling the Structure of Sputtered Tantalum Films", Fundamentals of Metal Deposition, Thin Solid Films, vol. 16, pp.129-143, 1973.

18. A. Schauer and W. Peters, "The Influence of Film Thickness on the Formation of β – Ta and BCC – Ta", Thin Solid Films, vol. 27, pp. 95-99, 1975.

19. Shigehiko SATO, "Nucleation Properties of Magnetron-Sputtered Tantalum", Thin Solid films, vol. 94, pp. 321-329, 1982.

20. R. D. Burbank, "An X-ray Study of Beta-Tantalum", J. Appl. Cryst., vol. 6, pp. 217-224, 1973.

21. R. B. Marcus and S. Quigley, "Formation of F. C. C., B. C. C. and β-Tantalum films by Evaporation", Thin Solid Films, vol. 14, no. 2, pp. 467-477, 1972.

22. P. N. Denbigh and R. B. Marcus, "Structure of Very Thin Tantalum and Molybdenum Films", J. Appl. Phys., vol. 37, no. 12, pp. 4325-4330, 1966.

23. G. Das, "A New Structure of Sputtered Tantalum", Thin Solid Films, vol. 12, pp. 305-311, 1972.

24. L. M. Hsiung and D. H. Lassila, "Shock Induced Omega Phase in Tantalum", Scripta Materialia, vol. 38, no. 9, pp. 1371-1376, 1998.

25. N. Schwartz and E. D. Feit, "Impurity Effects in the Nucleation of Alpha (bcc) – Tantalum or Beta – Tantalum Coatings", J. Electrochem. Soc., vol. 124, no. 1, pp. 123-131, 1976.

REFERENCES
(Continued)

26. H. C. Starck URL http://www.hcstarckus.com/main44.html (Sept. 19, 2000).

27. URL http://www.eecs.umich.edu/USL/MaterialScience/index.html (Dec. 6, 2000).

28. Douglas Chrisey and Graham Hubler, *Pulsed Laser Deposition of Thin Films*, John Wiley & Sons Inc., USA, 1994.

29. Klaus K. Schuegraf, *Handbook of Thin Film Deposition Processes and Techniques*, Noyes Publications, Park Ridge, NJ, 1988.

30. Brian Chapman, *Glow Discharge Processes*, John Wiley & Sons Inc., USA, 1980.

31. URL http://hypatia.dartmouth.edu/levey/ssml/equipment/SEM/SEM_intro.html (Nov. 28, 2000).

32. K. Hieber and N. M. Mayer, "Structural Changes of Evaporated Tantalum During Film Growth", Thin Solid Films, vol. 90, pp. 43-50, 1982.

33. S. L. Lee and D. Windover, "Phase, Residual Stress, and Texture in Triode-Sputtered Tantalum Coatings on Steel", Surface and Coatings Technology, vol. 108-109, pp. 65-72, 1998.